

Section 4

**Parameterization of important
atmospheric and surface processes,
effects of different parameterizations**

Computationally Fast and Accurate Surface Turbulent Fluxes

Mark A. Bourassa^{1,2} and Paul J. Hughes^{1,2}

(bourassa@coaps.fsu.edu and hughes@coaps.fsu.edu)

1. Center for Ocean-Atmospheric Prediction Studies, Florida State University, Tallahassee, FL 32306-2840, USA

2. Department of Meteorology, Florida State University, Tallahassee, FL 32306-4520, USA

1. INTRODUCTION

A theoretical, physically-based model (Bourassa 2006) is used to produce a lookup table for surface turbulent fluxes. The model and lookup table consider dependencies on wind speed, air-sea temperature differences, and directional wave characteristics. The physical impacts of sea state are parameterized through the influences of the surface's orbital motion induced by waves, as well as a vertical displacement of the log-wind profile (displacement height). The considerable input information is reduced to a three-dimensional lookup table. The grid is designed to allow for very rapid interpolation to the transfer coefficient for stress (the drag coefficient), latent heat (or moisture) flux, and the sensible heat flux. This model is well suited to use in applications where there are many calls to the surface flux code, such as numerical weather prediction model and ocean modeling.

2. MODEL PHYSICS

The theoretical flux model (Bourassa 2006) is a combination of the strengths of a variety of flux models. The low wind speed stress is similar to that of the BVW model (Bourassa et al. 1999), which considers three types of roughness elements: smooth surfaces, capillary waves, and gravity waves. The gravity wave part of that model had shortcomings that were dealt with through an improved parameterization of sea state influences (Bourassa 2004). That solution had shortcomings related to very high seas, which were corrected by considering displacement height (Bourassa 2006). The resulting model considered two influences of waves: a lower boundary condition on velocity, related to the orbital motion of the waves, and a vertical displacement related to wind waves. The resulting modeled stresses were well matched to observations from the Storm Wave Study experiment (SWS-2; Dobson et al., 1999; Taylor et al., 1999), which were kindly provided by Peter K. Taylor. The wind speeds in the SWS-2 observations ranged from 2 to 21 ms⁻¹ (after quality control), and included a wide range of wave conditions.

The modeled heat fluxes are based on the CFC model (Clayson et al. 1996). This model is founded on surface renewal theory. One parameter was adjusted to a more widely accepted value, correcting an underestimation of the roughness length. This adjustment, and the improved stress-related parameterizations, results in a much better match to high wind speed fluxes, correcting a known deficiency (M. Brunke, personal communication, 2002) of the CFC model.

3. FLUX MODEL EQUATIONS

The fluxes considered in this model are the downward momentum flux ($\boldsymbol{\tau}$), the upward surface turbulent fluxes of sensible (H), moisture (E), and latent heat (Q). Stress can be modeled in terms of the friction velocity (\mathbf{u}_*):

$$\boldsymbol{\tau} = \rho \mathbf{u}_* |\mathbf{u}_*|, \quad (1)$$

where ρ is the density of the air. Sensible heat, moisture flux, and latent heat are

$$H = -\rho C_p \theta_* |\mathbf{u}_*|, \quad (2)$$

$$E = -\rho q_* |\mathbf{u}_*|, \quad (3)$$

$$Q = -\rho L_v q_* |\mathbf{u}_*| = L_v E, \quad (4)$$

where θ_* and q_* are scaling parameters analogous to u_* , C_p is the specific heat of air, and L_v is the latent heat of vaporization.

The direct influence of surface waves on flux and airflow characteristics (\mathbf{u}_* and z_o) is determined by the relation between \mathbf{u}_* and roughness length (z_o). Given $z_o(\mathbf{u}_*)$ and the modified log wind relation $\mathbf{U}(z)$, where z is the height above the local mean surface, it is possible to iteratively solve for $\mathbf{u}_*(\mathbf{U})$ and $\boldsymbol{\tau}(\mathbf{U})$. The modified log-wind relation is

$$\mathbf{U}(z) - 0.8\mathbf{U}_{orb} - \mathbf{U}_{curr} = \frac{\mathbf{u}_*}{\kappa} \left[\ln \left(\frac{z - H_{wind}}{z_o} + 1 \right) + \phi(z, z_o, L) \right], \quad (5)$$

where k is von K arm an's constant, d is the displacement height (the height at which the log wind profile extrapolates to zero wind speed), and L is the

Monin-Obukhov stability length. The influence of atmospheric stratification in the boundary-layer is modeled through the Monin-Obukhov stability length (Liu et al., 1979). The profiles of potential temperature (θ) and specific humidity (q) have functional forms similar to the log-wind profile.

$$\theta(z) - \theta_s = \frac{Prt \theta_*}{k} \left[\ln \left(\frac{z}{z_{o\theta}} + 1 \right) + \varphi_\theta(z, z_{o\theta}, L) \right] \quad (6)$$

and

$$q(z) - q_s = \frac{Sct q_*}{k} \left[\ln \left(\frac{z}{z_{oq}} + 1 \right) + \varphi_q(z, z_{oq}, L) \right], \quad (7)$$

where Prt is the turbulent Prandtl number, and Sct is the turbulent Schmidt number. The parameters Prt and Sct are often used to tune the gain of flux models (i.e., $\partial E / \partial(q - q_s)$ and $\partial H / \partial(\theta - \theta_s)$). The parameterization of momentum roughness length is described in Bourassa (2006), and the roughness lengths for potential temperature ($z_{o\theta}$) and specific humidity (z_{oq}) are adapted from the surface renewal model of Clayson et al. (1996). The parameterization of L is identical to that used in the BVW (Bourassa-Vincent-Wood) flux model (Bourassa et al., 1999), the CFC (Clayson-Fairall-Curry) model (Clayson et al. 1996), and Bourassa (2003).

4. WAVE INFLUENCES ON FLUXES

One input to the model should be the wave-relative wind, in vector components, and the height corresponding to this wind. That is, the wind speed minus the current and the wave's orbital velocity. Many NWP models include wave information from which the orbital velocity of the dominant waves can easily be extracted. Assuming a value of zero for the orbital velocity results in slight overestimations of the fluxes. The observation height should also be modified by subtracting 80% of the height of the dominant wind waves. With these two considerations, the model accounts for directional wave influences on fluxes. In theory, this approach would also include changes in wave characteristics and fluxes associated with shallow water.

The wave data can often be ignored; however, this will introduce small biases, which might be important for climate modeling. For applications involving large waves, the wave considerations can be very important, and should not be ignored.

The model lookup tables are based on transfer coefficients, which the model combines with the input data to determine the surface turbulent fluxes. The lookup table is designed so that the lookup table indices can be determined with one computationally fast calculation for each index. Tri-linear interpolation

is used to interpolate between grid points. The three axes are surface relative wind speed, difference in atmospheric and surface potential temperature, and reference height relative to the wave disturbed surface. Note that the height considerations allow input data from between 2 and 40m.

5. ADDITIONAL FLUX MODEL INPUT/OUTPUT

Additional input requirements are a sea surface temperature, air temperature and specific humidity with the corresponding height corresponding to these observations, and surface pressure.

The model output data are vector stress components (Nm^{-2}), sensible heat flux (Wm^{-2}), and latent heat stress (Wm^{-2}).

6. CLOSING COMMENT

This lookup table version of the flux model is now used to product the FSU winds and fluxes. The analysis scheme highly iterative, particularly when used to objectively determine weighting parameters. The use of this new flux model resulted in an increase in processing speed, despite replicating a much more complex model of surface fluxes.

Acknowledgments. Support for the development of the lookup table is from NOAA OCO and the NSF. COAPS base funding is from NOAA/CDEP.

REFERENCES

- Bourassa, M. A., 2004: An Improved Seastate Dependency For Surface Stress Derived from In Situ and Remotely Sensed Winds. *Advances in Space Res.*, **33**(7), 1136-1142.
- Bourassa, M. A., 2006, Satellite-based observations of surface turbulent stress during severe weather. *Atmosphere - Ocean Interactions*, Vol. 2., ed., W. Perrie, Wessex Institute of Technology Press, 35 – 52 pp.
- Bourassa, M. A., D. G. Vincent, and W. L. Wood, A flux parameterization including the effects of capillary waves and sea state. *J. Atmos. Sci.*, **56**, 1123-1139, 1999.
- Clayson, C. A., C. W. Fairall, and J. A. Curry, 1996: Evaluation of turbulent fluxes at the ocean surface using surface renewal theory, *J. Geophys. Res.*, **101**, 28,503-28,513.
- Dobson, F. W., R. J. Anderson, P. K. Taylor, and M. J. Yelland, Storm Wind Study II: Open ocean wind and sea state measurements. *Proc. Symp. on the Wind-Driven Air-Sea Interface: Electromagnetic and Acoustic Sensing, Wave Dynamics and Turbulent Fluxes*, M. L. Banner, Ed., University of New South Wales, 295-296, 1999.
- Taylor, P. K., and M. J. Yelland, F. W. Dobson, R. J. Anderson, Storm Wind Study II: Wind stress estimates from buoy and ship. *Proc. Symp. on the Wind-Driven Air-Sea Interface: Electromagnetic and Acoustic Sensing, Wave Dynamics and Turbulent Fluxes*, M. L. Banner, Ed., University of New South Wales, 353-354, 1999.

A prognostic large scale cloud and semi-Lagrangian precipitation scheme in ARPEGE and ALADIN models

F. Bouysse, Y. Bouteloup, P. Marquet

Météo-France, CNRM/GMAP, 42 av. G. Coriolis, 31057 Toulouse Cedex, France.

The large scale precipitation and the cloudiness schemes used operationally at Météo- France in the global ARPEGE and limited area ALADIN numerical weather prediction (NWP) models for short range forecasting include no storage of liquid and solid water. The large scale precipitation occurs when water vapor is above wet bulb water vapor and falls in one time step. A revised Kessler method is used for computing precipitation evaporation, melting and freezing. The diagnostic scheme for the “radiative” clouds link the cloudiness to the production of stratiform and convective precipitations, and to the existence of inversions. The cloudiness functionally depends on the diagnosed total cloud condensate (Xu and Randall, 1996). Used operationally since many years, these schemes have proved their robustness and utility for short range forecasting. However the use of more sophisticated microphysics is promising for improving the simulation of clouds, precipitations and surface conditions. Therefore the large scale cloud and precipitation scheme developed by Lopez (2002) has been tested and improved to be used in ARPEGE and ALADIN models (Bouysse et al. 2005, Bouteloup et al. 2005).

Originally based on the addition of two prognostic quantities, namely the amount of cloud condensate (suspended liquid water plus ice) and the precipitation content (rain plus snow), the Lopez’s scheme is based now on the addition of four prognostic quantities: the amount of cloud liquid water, ice cloud water, rain and snow. A prognostic treatment of precipitation has been chosen to provide a finer description of the temporal evolution of the vertical distribution of precipitation (especially snow) and, thus, of the effects of latent- heat release associated with sublimation and evaporation. The calculations of large scale condensation/evaporation and cloud fraction are based on a triangular probability- density functions (Smith, 1990). The width of this function is adjusted via a critical relative humidity threshold, above which clouds start to appear. An analytical formulation has been designed to describe the dependency of “critical relative humidity” with height and horizontal resolution . The partitioning of stratiform cloud condensate into cloud liquid water and cloud ice is diagnosed from the local temperature. The parameterized microphysical processes that involve precipitation are autoconversion, collection, evaporation/sublimation and melting. The autoconversion rate of cloud droplets (ice crystals) into precipitating drops (snowflakes), is given by the simple formulation of Kessler. The threshold coefficient for autoconversion of cloud ice to snow is function of temperature. Three

types of collection processes are considered: accretion, aggregation and riming for which the classical continuous collection equation has been integrated over the Marshall-Palmer exponential particle spectra for specified distributions of particle fall speed and mass. Precipitation evaporation is calculated by integrating the equation that describes the evaporation of a single particle over the assumed spectra of particle number, mass, and fall speed. The fall of rain and snow are considered as specific processes, and are computed using a semi-Lagrangian approach, valid for the long NWP and GCM time-steps, that is separate from the standard semi-Lagrangian advection scheme used in ARPEGE and ALADIN models.

The scheme has been validated with an improved turbulence scheme which diffuses cloud conservative variables (moist static energy and total water content) and the operational ECMWF radiation scheme. These modifications are currently in pre-operational tests for weather forecasting and climate simulation with ARPEGE and ALADIN models. The benefits are an improvement of cloud representation (more high clouds and less medium clouds). The amount of precipitation is smoother spatially, with more precipitation on the leeward mountains and less on the windward mountains, both aspects being beneficial according to the current model biases. The use of a prognostic microphysics is expected to be also beneficial for the future assimilation of cloud satellite radiances and radar reflectivities, and the coupling of the future operational high resolution model (AROME).

Bouysse, F., Y. Bouteloup, P. Marquet, 2005: Towards an operational implementation of Lopez's prognostic large scale cloud and precipitation scheme in ARPEGE/ALADIN NWP models. HIRLAM/ALADIN workshop proceedings on convection and clouds, pp 56-60.

Bouteloup, Y., F., Bouysse, P. Marquet, 2005: Improvements of Lopez's prognostic large scale cloud and precipitation scheme. ALADIN Newsletter 28, pp 66-73.

Lopez, P., 2002: Implementation and validation of a new prognostic large-scale cloud and precipitation scheme for climate and data-assimilation purposes. Q. J. R. Meteorol. Soc., 128, 229-257.

Smith, R. N. B., 1990: A scheme for predicting layer clouds and their water content in a general circulation model. Q. J. R. Meteorol. Soc., 116, 435-460.

Xu, K.M. and D. Randall, 1996: A semi-empirical cloudiness parameterisation for use in climate models. J. Atmos. Sci., 53, 3084-3102.

The Response of the Terrestrial Biosphere and the Global Mean $\delta^{18}\text{O}$ Value of Atmospheric CO_2 to Humidity Changes

Nikolaus Buenning¹, David Noone¹, William Riley², Christopher Still³, James Randerson⁴, and Lisa Welp⁵

¹*Department of Atmospheric and Oceanic Sciences and Cooperative Institute of Research in Environmental Sciences, University of Colorado, Boulder, CO, USA*

²*Earth Sciences Division Lawrence, Berkeley National Laboratory, Berkeley, CA, USA*

³*Geography Department, University of California, Santa Barbara, CA, USA*

⁴*Department of Earth System Science, University of California, Irvine, CA, USA*

⁵*Environmental Science and Engineering, California Institute of Technology, CA, USA*

(Email: buenning@colorado.edu)

The atmospheric concentration of CO^{18}O is largely influenced by the terrestrial biosphere through respiration and photosynthetic leaf fluxes. Both the gross CO_2 exchange and the isotopic composition of leaf and soil water influence the isotopic leaf and soil fluxes that affect the composition of ^{18}O in CO_2 (denoted hereafter as $\delta^{18}\text{O} = (\text{R}/\text{R}_{\text{Standard}} - 1) \times 1000$, where R is the mole ratio of heavy to light isotopes). Craig and Gordon (1965) showed under the approximation of steady state conditions and constant leaf water volume, the leaf water isotope ratio of $\text{H}_2^{18}\text{O}/\text{H}_2^{16}\text{O}$ at the evaporation site is related to humidity such that it is most enriched in the heavy oxygen isotope at low humidity and is most depleted at 100% relative humidity. Soil water is also able to become enriched when the evaporation rate is high, which again is related to the relative humidity of the atmospheric surface layer. Because of this, the $\delta^{18}\text{O}$ value of CO_2 may be a sensitive indicator of the global hydrologic cycle. Using model simulations, we investigate how changes in relative humidity can affect the isotopic state of the terrestrial water pools and atmospheric CO_2 .

The isotopic version of the NCAR Land Surface model (ISOLSM, Bonan, 1996; Riley et al., 2002) was used to simulate the isotopic state of the leaf and soil water pools and CO_2 fluxes. Conserving both water and energy, ISOLSM simulates the water and carbon exchanges, and uses kinetic and equilibrium fractionation to account for ^{18}O . The model is forced with meteorological data from the NCEP reanalysis, and the $\delta^{18}\text{O}$ value of precipitation and water vapor are prescribed from the MU-GCM monthly climatology (Noone and Simmonds, 2002). To simulate the $\delta^{18}\text{O}$ value of CO_2 , the monthly mean balanced surface CO_2 fluxes from ISOLSM are inputted into the NCAR Community Atmosphere Model (CAM). The ocean fluxes are prescribed monthly means calculated from pCO_2 differences between the ocean and the marine atmosphere (Takahashi et al., 1997). All CO_2 fluxes and surface CO^{18}O fluxes are prescribed monthly means. However CO^{18}O fluxes from the atmosphere to the surface are dependent on the ratio of $\text{CO}^{18}\text{O}/\text{CO}_2$, such that a global equilibrium of $\delta^{18}\text{O}$ in CO_2 is reached. To examine how relative humidity changes affect both the isotopic composition of the terrestrial water pools and atmospheric CO_2 , two experiments were performed that reduced the prescribed relative humidity to 90% and 80% of its original value. For these two experiments, the $\delta^{18}\text{O}$ of water vapor is fixed and not allowed to adjust dynamically with the leaf water.

The results of these two experiments suggest that there is a strong dependence of relative humidity on the isotopic composition of the leaf and soil water, omitting latitudes

without vegetation (Figure 1). When the relative humidity is reduced to 80% of its original value the zonal mean of the soil water becomes more enriched by about 0.0%-3.0%. The zonal mean of the leaf water becomes even more enriched (2.0-7.0%), due to the enriched soil water, decreased humidity, and enrichment occurring in the leaf itself.

When relative humidity is reduced to 90% and 80% of its original value, the $\delta^{18}\text{O}$ value of CO_2 becomes enriched globally by 1.3‰ and 3.0‰, respectively. Noting that observations show typical variability in the range of 1-2‰, these results suggest that small changes in global relative humidity could have a substantial impact on the $\delta^{18}\text{O}$ value of CO_2 . Specifically, a global deviation of 0.5‰ (as seen in observations) would require a humidity change in the most productive regions of only 3% based on model results. This largely confirms that the $\delta^{18}\text{O}$ value of CO_2 provides an integrated metric of the global hydrologic cycle.

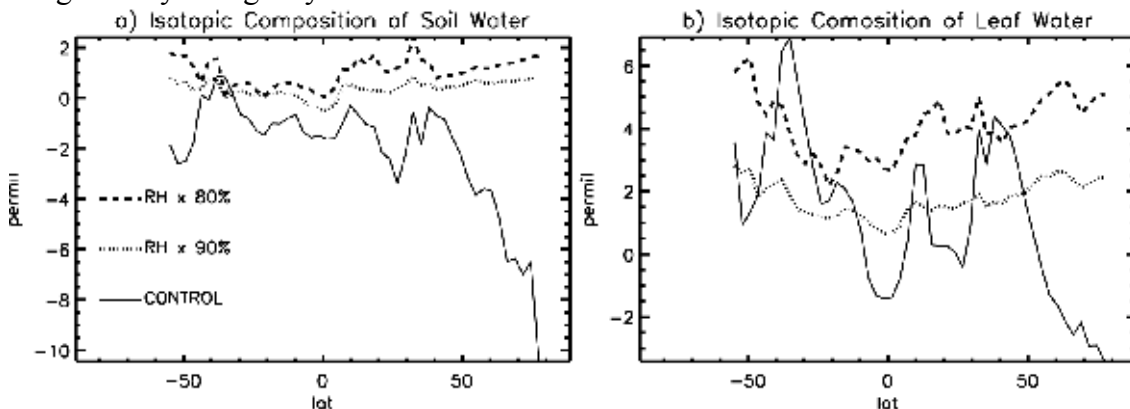


Figure 1. Zonal mean $\delta^{18}\text{O}$ of photosynthesis-weighted soil (a) and leaf (b) water for the control simulation (solid line). The experiments that reduce the relative humidity to 90% (dotted line) and 80% (dashed line) of its original value are plotted as experiment minus control.

References:

- Craig, H., and Gordon A., 1965. Deuterium and Oxygen-18 variations in the ocean and the marine atmosphere. In: *Stable isotopes in oceanic studies and paleotemperatures* (ed. Laboratory of Geology and Nuclear Sciences), Pisa, Italy.
- Bonan, G., 1996: A land surface model (LSM version 1.0) for ecological, hydrological, and atmospheric studies: Technical description and user's guide, TN-417+STR, Natl. Cent. For Atmos. Res., Boulder, CO.
- Noone, D., and Simmonds, I., 2002: Associations between $\delta^{18}\text{O}$ of water and climate parameters in a simulation of atmospheric circulation for 1979-1995. *J. Climate* **15**(22), 3140-3169.
- Riley, W. J., Still, C. J., Torn, M., and Berry, J. A., 2002: A mechanistic model of H_2^{18}O and C^{18}OO fluxes between ecosystems and atmosphere: model description and sensitivity analyses. *Global Biogeochem. Cycles* **16**, 1095-1108.
- Takahashi, T. Feely, R. A., Weiss, R. F., Wanninkhof, R. H., Chipman, D. W., Sutherland, S. C., Takahashi, T. T. 1997. Global air-sea of CO_2 : An estimate base on measurements of sea-air pCO_2 differences. *Proc. Natl. Acad. Sci. USA* **94**, 8292-8299.

Towards urbanisation of the non-hydrostatic numerical weather prediction model Lokalmodell (LM)

Barbara Fay, Lina Neunhäuserer, Matthias Raschendorfer
Deutscher Wetterdienst, P.O.Box 106465, D-63004 Offenbach am Main, Germany

With a growing part of the world population living in cities and increasing air pollution abatement legislation (e.g. recently enforced European Union air quality regulations), the need for forecasts of local pollutant concentration rises. Urban air quality forecasting is investigated or operational in many large European cities also using an increasing number of nested high-resolution NWP models. This topic was also advanced in the European FP5 project FUMAPEX (Integrated Systems for Forecasting Urban Meteorology, Air Pollution and Population Exposure, 2002-2005, <http://fumapex.dmi.dk>) with participation of the DWD.

The urban boundary layer is characterised by a more complex structure than the rural one. Building complexes and street canyons form the urban canopy layer as part of the horizontally inhomogeneous and non-equilibrium surface boundary layer where the Monin-Obukhov similarity theory (MOST) used in most current operational NWP models is invalid and cannot reproduce the measured vertical structure of the turbulence field in the urban roughness sublayer (Rotach, 1995, Fisher et al., 2005). Initial model urbanisation steps include urbanised physiographic parameters and an anthropogenic heat source in the NWP models. Advanced measures consist of the introduction of urban surface layer schemes parameterising the urban canopy and roughness layer (e.g. Martilli et al., 2002).

First urbanisation steps were applied to the Lokalmodell LM by introducing urbanised physiographic parameters and an anthropogenic heat source (Neunhäuserer and Fay, 2005). The definition of a soil type 'city' along with corresponding changes of albedo, thermal conductivity and capacity according to Kinouchi et al. (2001) and of improved surface roughness, plant cover and leaf area index influence the surface heat and water budgets and the dynamics. Optionally, an anthropogenic heat source of 20 or 60W/m² was added to the surface energy balance (Best and Betts, 2004). A sensitivity study was performed for the Helsinki spring dust episode around 10 April 2002 above an enlarged and all-concrete city centre (results of LM episode evaluation and model inter-comparison for high-resolution NWP models with up to 1km resolution in Fay and Neunhäuserer, 2005; Fay et al., 2004 and 2005). The main differences in surface and 2m temperatures can be attributed to the urbanised physiographic parameters during the day while the impact of the anthropogenic heat flux rises at night (up to 7°C in surface temp compared to the non-urbanised version), partly due also to the initially assumed constant anthropogenic flux. Thus, a distinct urban heat island effect and more characteristic urban fluxes were achieved. Comparison with measurements show improved model results compared with measurements (Fig. 1 left). The components of the urban storage heat flux were also analysed separately. The change in physiographic parameters leads to a considerable shift in the partitioning of the heat fluxes during the day, with an increase of the sensible and a decrease of the latent heat fluxes reflecting urban observations. The storage heat flux is mainly negative during the day, indicating an increased energy intake of the urban texture increased soil temperature, and a slightly positive upward storage heat flux into the atmosphere for the following night (Fig. 1 middle). An added (continuous and constant) anthropogenic heat flux is generally split between sensible heat flux and storage heat flux, with the sensible heat flux prevailing during the day and warming the atmosphere and the storage heat flux dominating through the night and increasing the soil and surface temperature (Fig. 1 right).

Further sensitivity studies were performed concerning urban effects (e.g. the hysteresis loop described by Grimmond et al., 1999), refined physiographic parameters and a time-variant anthropogenic heat flux. The full results are described in Neunhäuserer et al. (2006).

The introduction of even simple urbanisation measures in LM thus leads to a distinct urban heat island effect and urbanised surface fluxes (increased Bowen ratio and heat storage). Further improvements are expected by refining these measures and by the introduction of the generalised high-resolution parameterisation scheme of LM under development at the DWD that will also be suitable for the urban canopy and roughness layer. The urban canopy layer parameterisation by Martilli et al. (2002) has

recently been included into the Swiss LM version aLMo during the FUMAPEX project. Further LM studies are planned for a German government-funded research project on megacities.

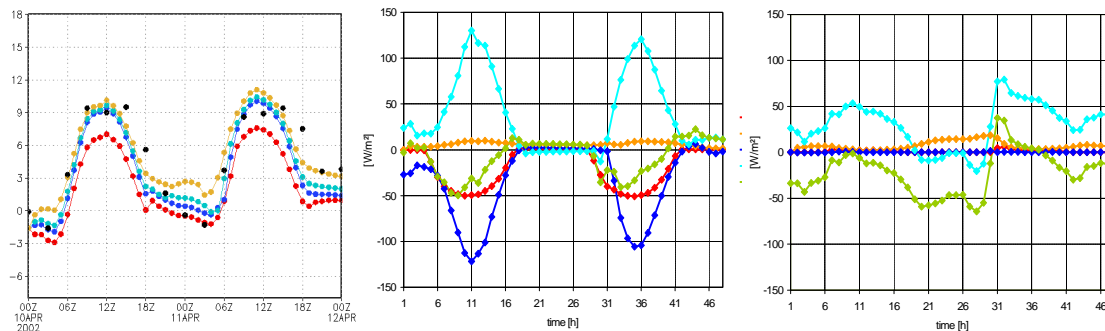


Fig. 1. Urbanised LM 1.1km, 48 time series at Helsinki,Kaisaniemi, starting 10 Apr 2002, 00UTC+00. Left: 2m temperature ($^{\circ}\text{C}$), red=orig. LM, blue=urbanised physiographic param., turquoise=blue plus $20\text{W}/\text{m}^2$ anthropog. heat source, yellow=blue plus $60\text{W}/\text{m}^2$. Middle: Differences in radiation and fluxes for case(urbanised physiographic parameters)-case(non-urb.LM). Right: Differences in radiation and fluxes for case(urbanised phys. param. plus $60\text{W}/\text{m}^2$ anthrop. heat source)-case(only urbanis. phys. param.). Middle and right: red=short wave radiation, orange=long wave rad., blue=lat. heat flux, turquoise=sens. heat flux, green=storage heat flux.

Acknowledgements

This study is part of the EU FP5 project FUMAPEX (Integrated Systems for Forecasting Urban Meteorology, Air Pollution and Population Exposure, 2002-2005), funded by the EU under contract no. EVK4-CT-2002-00097. The authors thank their DWD colleagues in NWP modelling for valuable discussions and support.

References

- Best, M. and Betts, R. (2004) The impact of climate change on our cities. The 84th AMS Annual Meeting, Joint Session 5 Climate Change and Urban Areas, Seattle, WA, 15 Jan 2004.
- Fay, B., L. Neunhuserer, J.L. Palau, J.J. Dieguez, V. Oedegaard, N. Bjergene, M. Sofiev, M. Rantamaki, I.Valkama, J. Kukkonen, A. Rasmussen, A. Baklanov (2004) Model simulations and preliminary analysis for three air pollution episodes in Helsinki. FUMAPEX Report D3.3, DWD, Offenbach, Germany, 60pp.
- Fay, B., L. Neunhuserer, J.L. Palau, G. Perez-Landa, J.J. Dieguez, V. Oedegaard, G. Bonafe, S. Jongen, A. Rasmussen, B. Amstrup, A. Baklanov, U. Damrath (2005) Evaluation and inter-comparison of operational mesoscale models for FUMAPEX target cities. FUMAPEX Report D3.4, DWD, Offenbach, Germany, 110pp.
- Fay, B. and L. Neunhuserer (2005) Evaluation of very high-resolution simulations with the non-hydrostatic numerical weather prediction model Lokalmodell for urban air pollution episodes in Helsinki, Oslo and Valencia. *Atm. Chem. and Phys. Discussions*, 5, 8233-8284, 2005, www.atmos-chem-phys.org/acpd/5/8233/
- Fisher, B., Kukkonen, J., Piringer, M., Rotach, M.W. and Schatzmann, M. (2005) Meteorology applied to urban air pollution problems: concepts from COST715. *Atmos. Chem and Physics Discussions* 5, pp. 7903-7927.
- Grimmond, C.S.B. and Oke, T.R. (1999) Heat Storage in Urban Areas: Local Scale Observations and Evaluation of a Simple Model. *J. of Appl. Met.* 38, 922-940.
- Kinouchi, T. and Yoshitani, J.(2001) Simulation of the urban heat island in Tokyo with future possible increases of anthropogenic heat, vegetation cover and water surface. *Proc.2001 Int. Symp. on Environ. Hydraulics*, 6pp.
- Martilli, A., Clappier, A., Rotach, M.W.(2002) An urban surface exchange parameterisation for mesoscale models. *Bound. Lay. Met.*, 94, 357-397.
- Neunhuserer, L., Fay, B. (2005) Towards predicting urban air pollution episodes: Introduction of urbanised parameters into the mesoscale Lokalmodell (LM) of the German Weather Service. *Proceedings 5th Int. Conf. on Urban Air Quality*, Valencia, Spain, 29-31 Mar 2005, 4pp.
- Neunhuserer, L., Fay, B., Raschendorfer, M. (2006) Towards urbanisation of the non-hydrostatic numerical weather prediction model Lokalmodell (LM). Submitted to *Bound. Layer Met*, Jan 2006.
- Rotach, M.W. (1995) Profiles of turbulence in and above an urban street canyon. *Atm. Environ.*, 29, 1473-1486.

Sensitivity of the seasonal cycle simulated by a RCM to physical parameterizations

Jesús Fernández¹, Juan Pedro Montávez², Jon Saénz³, Jesús Fidel González-Rouco⁴ and Eduardo Zorita¹

¹ GKSS Forschungszentrum, Institute for Coastal Research, Geesthacht, Germany

² University of Murcia, Dept. of Physics, Murcia, Spain

³ University of the Basque Country, Dept. of Applied Physics II, Leioa, Spain

⁴ Complutense University of Madrid, Dept. of astrophysics and atmospheric sciences, Madrid, Spain

E-mail: Jesus.Fernandez@gkss.de

The sensitivity of the MM5 mesoscale modelling system [Grell et al., 1994] to the selection of the wide range of different physical parameterizations provided (including some of the most common schemes also used in global atmospheric models) is analyzed in terms of their ability to reproduce the seasonal cycle of precipitation and surface temperature over the Iberian Peninsula [Fernández et al., 2006].

The experiment was carried out by simulating the 5-year period 1985-1989 by nesting the MM5 model into the NCEP/NCAR Reanalysis [Kalnay et al., 1996] gridded data. The model was set up with two nests to get to 45 km resolution over an Iberian domain through a coarse mother domain covering the Atlantic/Mediterranean area with 135 km resolution. Two-way nesting was applied to allow feedback from the Iberian domain to the mother domain. Grid nudging to the Reanalysis data was applied to the mother domain over the boundary layer to keep the large scale circulation close to the observed one.

We designed 16 experiments by combining the physical parameterizations shown in the table below:

Microphysics	Cumulus	PBL	Radiation
Simple Ice	Grell	MRF	Cloud
Mixed-Phase	Kain-Fritsch	Blackadar	RRTM

where the first row corresponds with parameterizations using simpler assumptions (computationally more efficient) and the second with those using more sophisticated schemes. Details of the different parameterizations can be found in [Grell et al., 1994] and the references therein.

For validation purposes, precipitation (from González-Rouco et al. [2001]) and surface temperature (from the meteorological institutes of Spain and Portugal) station data were used. Other precipita-

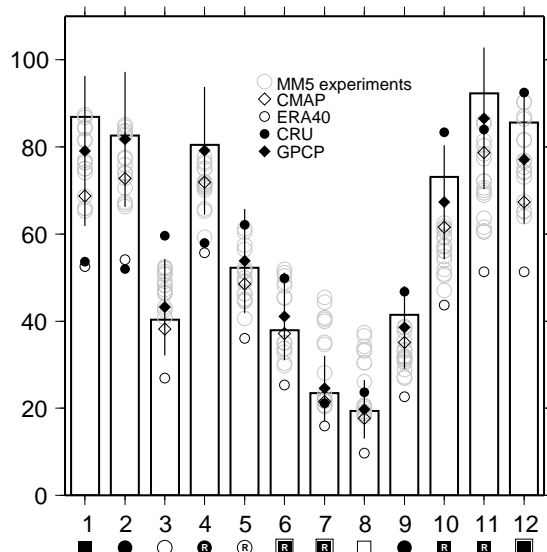


Figure: Area-averaged monthly seasonal cycle of precipitation according to the precipitation stations (bars), the 16 MM5 experiments, CPC Merged Analysis of Precipitation (CMAP), ERA40 precipitation at 2.5 degrees resolution, Global Precipitation Climatology Project (GPCP) which provides error estimates (also shown) and the Climatic Research Unit (CRU) 0.5 gridded data. Every data set is first bilinearly interpolated to the UCM stations and then averaged to avoid errors arising from the different coverage density of the UCM stations.

tion data sets (CMAP, ERA40, CRU and GPCP – see Figure) were used to analyze the observational uncertainty.

The overall performance of the model in capturing the area-average annual cycle of precipitation and surface temperature is good, although a bias towards cooler than observed temperatures was found. Particular features of the period selected, such as the strong april and low march precipitation, were well represented. The seasonal cycle in certain areas, however, presents bias. Precipitation is overestimated over the northern Iberian Peninsula and temperatures are underestimated especially in summer over the southeast.

The performance of the individual experiments is influenced by these biases. Experiments yielding higher temperatures perform better due to the cold bias. The experiments producing less rainfall are better in the northern interior Iberian Peninsula, where there is a positive bias. Moreover, no experiment is found to perform better than the others for every place, variable and season. The study, however, provides useful guidance on the selection of parameterizations for smaller subregions and for a specific variable and season.

Acknowledgements. Support for this research has been provided by the Basque Autonomous Government through grant BFI04.52, the University of the Basque Country (9/UPV 00060.310-15343/2003) and the Spanish Ministry of Science and Education (CGL2005-06966-C07-05/CLI).

References

- J. Fernández, J. P. Montávez, J. Sáenz, J. F. González-Rouco, and E. Zorita. Sensitivity of MM5 mesoscale model to physical parameterizations for regional climate studies: Monthly seasonal cycle. *J. Geophys. Res.*, 2006. Submitted.
- J. F. González-Rouco, J. L. Jiménez, V. Quesada, and F. Valero. Quality control and homogeneity of precipitation data in the Southwest of Europe. *J. Climate*, 14:964–978, 2001.
- G. A. Grell, J. Dudhia, and D. R. Stauffer. A description of the fifth-generation Penn State/NCAR Mesoscale Model (MM5). Technical Report NCAR/TN-398+STR, National Center for Atmospheric Research, 1994.
- E. Kalnay, M. Kanamitsu, R. Kistler, W. Collins, D. Deaven, L. Gandin, M. Iredell, S. Saha, G. White, J. Woollen, Y. Zhu, M. Chelliah, W. Ebisuzaki, W. Higgins, J. Janowiak, K. C. Mo, C. Ropelewski, J. Wang, A. Leetmaa, R. Reynolds, R. Jenne, and D. Joseph. The NCEP/NCAR 40-year Reanalysis Project. *Bull. Amer. Meteor. Soc.*, 77:437–471, 1996.

An intermediate solution between diagnostic exchange coefficients and prognostic TKE methods for vertical turbulent transport.

Jean-François Geleyn, Czech Hydrometeorological Institute, Prague, Czech Republic (*)
 Filip Vana, Czech Hydrometeorological Institute, Prague, Czech Republic
 Jure Cedilnik, Environmental Agency of Slovenia, Ljubljana, Slovenia
 Martina Tudor, Croatian Meteorological and Hydrological Service, Zagreb, Croatia
 Bart Catry, Ghent University, Ghent, Belgium
 (*) on leave of absence from Météo-France / email: Jean-Francois.Geleyn@chmi.cz

Method: It is often claimed that searching the stationary solution of a full prognostic Turbulent Kinetic Energy (TKE) scheme should in principle give a computation for vertical turbulent exchange coefficients close to that of schemes simply inferring those coefficients from the local vertical gradients of wind and potential temperature. We implicitly refer here either to the methods solving the Monin-Obukhov (MO) implicit set of equations or to those using a local Richardson number, in the wake of the Louis (1979) paper. To our knowledge however, there has never been an attempt to inverse the proposal, i.e. to find the TKE prognostic equations that would have for stationary solution some already computed exchange coefficients K_m (for momentum) and K_h (for energy).

This note aims at this unexplored goal. Said differently, given an already well tuned scheme delivering ‘static’ vertical exchange coefficients, how can one introduce in the simplest possible way the missing physical items that are advection, TKE vertical ‘auto-advection’ and balance between production-destruction on one hand and dissipation on the other hand? This problem could be attacked from several angles but its trademark is to search a common ground between TKE and MO-type methods. Since this is exactly what Redelsperger *et al.* (2001) (thereafter RMC01) did for creating a smooth transition between the upper-air behaviour of a ‘full’ TKE scheme and surface similarity laws, we elected to just adapt their method to the whole depth of the atmosphere. For this, an a-priori knowledge of the ‘stationary’ coefficients just replaces the choice of the MO functions. The procedure symbolically reads:

$$\tilde{K}_m, \tilde{K}_n \Rightarrow \tilde{K}_* \Rightarrow \tilde{E}, K_E, \tau_\varepsilon \quad (1)$$

$$dE/dt = f(E, \tilde{E}, K_E, \tau_\varepsilon) \quad (2)$$

$$E \Rightarrow K_* \quad (3)$$

$$K_*, \tilde{K}_*, \tilde{K}_m \ \& \ \tilde{K}_h \Rightarrow K_m \ \& \ K_h \quad (4)$$

where tilded values refer to the ‘static’ part of the computations and non-tilded ones to the prognostic aspects (including the last step of vertical exchange using the Equation (4) values of K_m and K_h , something which will not be detailed here, since being unchanged in the procedure). E is the TKE, K_E the auto-diffusion coefficient and τ_ε the relaxation time scale of the dissipation process (E/ε). K_n is the neutral state equivalent of K_m while K_* is a coefficient co-dimensional to K_m and K_n which we define as being the mirror image of E in case the equations at neutrality would be applicable for the whole range of stability conditions. Hence our problem is split into two parts: (i) solving the problem at neutrality and (ii) finding an expression to compute K_* from K_m and K_n , knowing that we shall then finish the exercise by using:

$$K_m = K_*(\tilde{K}_m/\tilde{K}_*) \ \& \ K_h = K_*(\tilde{K}_h/\tilde{K}_*) \quad (5)$$

Coming back to the problem at neutrality, it writes (RMC01):

$$\frac{dE}{dt} = A_{dv}(E) + \frac{1}{\rho} \frac{\partial}{\partial z} \rho K_E \frac{\partial E}{\partial z} + \frac{1}{\tau_\varepsilon} (\tilde{E} - E) \quad (6)$$

$$K_* = C_K L_K \sqrt{\tilde{E}} = C_K A_K \frac{l_m}{\kappa} \sqrt{\tilde{E}} \Leftrightarrow \tilde{E} = \left(\frac{\kappa \tilde{K}_*}{C_K A_K l_m} \right)^2 \quad (7)$$

$$K_E = \alpha K_* \quad (8)$$

$$\frac{1}{\tau_\varepsilon} = \frac{C_\varepsilon \sqrt{\tilde{E}}}{L_\varepsilon} = \frac{C_\varepsilon \kappa \sqrt{\tilde{E}}}{A_\varepsilon l_m} \quad (9)$$

with κ the Karman constant and l_m the static-scheme-type mixing-length for momentum, not to be confused with the TKE-type mixing-lengths $L_{K/\epsilon}$. As already hinted at, the last term of the first above equation represents a simple version of the balance between shear plus buoyancy production-destruction and dissipation, the Newtonian time scale being the one of the dissipation in the ‘full’ TKE formalism. In order to match these various aspects we have (RMC01, only near the surface in their case):

$$A_K = \frac{1}{\sqrt{\alpha}} \frac{\kappa}{C_K} \quad \& \quad A_\epsilon = \alpha \sqrt{\alpha} \kappa C_\epsilon \quad (10)$$

and (RMC01 again) we want $A_K = A_\epsilon$. Then, introducing ν with

$$C_K C_\epsilon = \frac{1}{\alpha^2} = \nu^4 \quad (11)$$

we finally get the very simple set of equations:

$$K_* = \nu l_m \sqrt{E} \Leftrightarrow \tilde{E} = \left(\frac{\tilde{K}_*}{\nu l_m} \right)^2, \quad K_E = \frac{l_m \sqrt{E}}{\nu}, \quad \frac{1}{\tau_\epsilon} = \frac{\nu^3 \sqrt{E}}{l_m} \quad (12)$$

where literature-reported measurements seem to indicate a value of 0.52 as the optimal one for ν .

Furthermore, studying the stability dependence of the various terms of the above equations and following again the guidelines of RMC01, it appears that $K_* = \sqrt{K_m K_n}$ is a good approximation of the ‘observed’ implicit behaviour of K_* .

Results: The scheme was implemented (in research mode) in the so-called CE version of the ALADIN NWP model. It gives either neutrality or slightly improved wind scores at the top of the PBL, leads to a reasonable distribution of E -values and appears rather stable. But its main advantage is probably its capacity to separate numerical stability problems (already treated, see below), choice of adequate mixing length values and the encompassing in \tilde{E} and in K_* of all the needed information about the functional dependency of the production-destruction mechanisms (i.e. more sophisticated formulae for the latter could mimic the intrinsic ‘physics’ of complex ‘full’ TKE schemes, without changing the numerical framework).

Discussion: Apart from the just mentioned flexibility-modularity issue, there are other advantages in this way of formulating the problem. In case of a potentially stiff behaviour of the diffusion equations in the vicinity of the neutral state, a so-called ‘anti-fibrillation’ specific treatment (alike the one of Bénard *et al.*, 2000) can be applied to the computation of the tilded value, something impossible in a fully prognostic TKE scheme. The scheme is naturally discretised in a way that allows to have the E -values in the middle of the model layers, this facilitating a semi-Lagrangian handling of the advection term common with that of other prognostic variables, a quite important practical advantage. Of course the vertical staggering with respect to the K -values (at the layers’ interfaces) might create a spurious vertical mode. But inspection of the last two Equations of (12) shows that the welcome local proportionality between K_E and $1/\tau_\epsilon$ allows to curb this danger through the choice of big enough values of l_m (and hence of L) with respect to the layer’s thicknesses.

The proposed scheme has a few common points with the one of Brinkop and Roeckner (1995) but, apart from its reliance on the computation of \tilde{K}_m and \tilde{K}_h , (i) it allows to decouple the intensities of diffusion and auto-diffusion, (ii) it treats separately the two types of stability dependence and (iii) it does not require the change of variable in (\sqrt{E}) to offer a numerically stable solution.

Bénard, P., A. Marki, P. N. Neytchev and M. T. Prtenjak, 2000, *Mon. Wea. Rev.*, **128**, pp. 1937-1948.

Brinkop, S. and E. Roeckner, 1995, *Tellus*, **47A**, pp. 197-220.

Louis, J.-F., 1979, *Boundary-Layer Meteorol.*, **17**, pp. 187-202.

Redelsperger, J.-L., F. Mahé and P. Carlotti, 2001, *Boundary-Layer Meteorol.*, **101**, pp. 375-408.

Advances in the integration of deep convection and microphysics for the meso-scale

Luc Gerard*, Jean-Marcel Piriou⁺, Jean-François Geleyn[°].

(*) *Royal Meteorological Institute of Belgium, Luc.Gerard@oma.be*

(⁺) *Météo-France/CNRM, ([°]) Czech Hydrometeorological Institute*

The foremost phenomenon driving the formation of clouds is the local saturation of moist air. Its correct evaluation relies on that of the local moisture, temperature and pressure. It has been a long practice in operational numerical weather prediction models to split it between a ‘resolved’ part (i.e. which can be considered ‘homogeneous’ when seen at the scale of the grid box), associated to stratiform or frontal events and a ‘subgrid’ part, linked to deep convection. For the ‘resolved’ part, statistical considerations can be used to evaluate the effect of the smaller scale features; this is the starting point of most microphysical packages. However, at all resolutions with grid boxes greater than 2 or 3 km, the effects of deep convective systems cannot be represented satisfactorily without a dedicated scheme, which is often a mass flux scheme. Combining the output of this scheme – condensation, precipitation, cloudiness – with the main microphysical scheme is not straightforward.

The problem is especially acute when the grid-box length lies between 7 km and 2 km, so that the convective clouds are partly resolved, partly subgrid. This is now often referred to as a ‘grey zone’ of resolutions, which ‘should be avoided’. Still, these intermediate resolutions are interesting in many circumstances. Moreover, having a scheme which results are not dependent of the resolution thanks to a smooth combination of resolved and subgrid parts represents a considerable advance.

The core of our solution is a cascading approach of the processes which have an impact on moisture and water contents. In our scheme, these are the turbulent diffusion, the resolved condensation, the convective updraught, the generation and the growth of precipitation by microphysical processes, its evaporation, and a moist downdraught. Each of them uses as input state values of temperature and phase contents modified by the action of the previous one. The update is done in such a way that the processes participating to the closure of the mass flux schemes (updraught and downdraught) are not included in it, to avoid double counting.

The deep convection scheme was adapted from the one described in GERARD and GELEYN [2005] (mass flux scheme with prognostic variables for updraught vertical velocity and mesh fraction). It has been completed to detrain cloud condensates instead of directly producing precipitation. Another difference is that it impacts on the mean grid-box variables through convective condensation fluxes (to ice and to liquid) and convective transport fluxes (of water species, heat and momentum).

The condensates which detrain from the updraught are combined with those produced by resolved condensation, before entering the microphysical package.

The figures below show an episod of intense thunderstorm over Belgium on 10 September 2005. The benefit of running at 4-km grid-length is significant.

The tests at different resolutions (10, 7, 4 and 2.2 km) show a smooth transition of the 1-hour accumulated surface precipitation field, which increases regularly, yielding more

precise patterns with increasing resolution. The amounts increase because of a better rain/no rain separation, but also because the correlation between high moisture and low temperature is more finely represented.

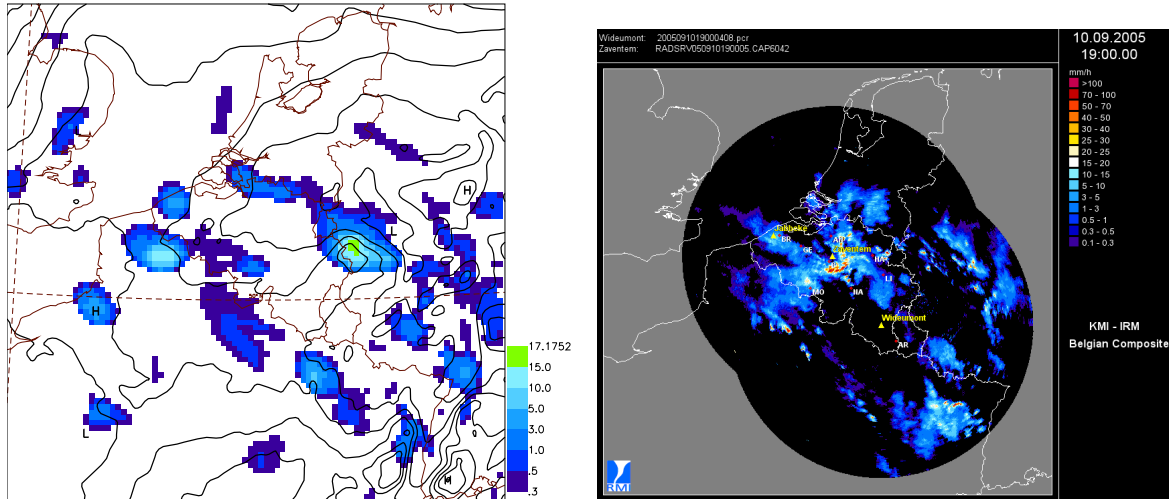


Figure 1 : Left: forecast at 7-km resolution, integrated scheme. Mean sea-level pressure (hPa), 1-hour accumulated precipitation (mm) at 19:00 utc. Right: Instantaneous radar reflectivities at 19:00 utc

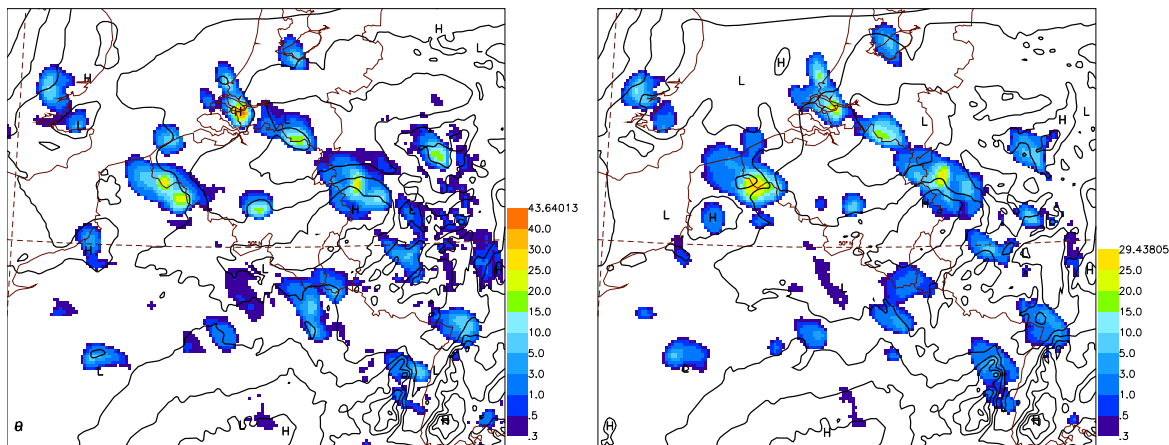


Figure 2 : Forecast at 4-km resolution. Mean sea-level pressure (hPa), 1-hour accumulated precipitation (mm) at 19:00 utc. Left: integrated scheme. Right: large scale scheme alone, with the convective scheme switched off.

References

L. GERARD and J.-F. GELEYN. Evolution of a subgrid deep convection parametrization in a limited area model with increasing resolution. *Q.J.R. Meteorol. Society*, 131:2293–2312, 2005.

PDF Cloud Scheme and Prognostic Cloud Scheme in JMA Global Model

Hideaki KAWAI*

Climate Prediction Division, Japan Meteorological Agency, Tokyo, Japan

1 Background

JMA (Japan Meteorological Agency)/MRI (Meteorological Research Institute) unified global model GSM (Global Spectral Model) is utilized not only for operations but also for climate researches including global warming simulations and will be used for operational ENSO predictions as a part of a coupled model in the near future. Therefore cloud scheme in GSM should represent large scale condensation precipitation appropriately, complicated cloud processes should be parameterised as properly as possible and the bias on radiation flux must be small for such a large variety of uses.

A PDF (Probability Distribution Function) cloud scheme (Sommeria and Deardorff 1977) is used in the current GSM. The PDF scheme in GSM is similar to Smith (1990), though so-called top hat type PDF is adopted in GSM. But some problems are recognized in PDF cloud schemes especially when these are utilized in large grid models such as global models. The most serious problem is discussed in Wood and Field (2000) and they showed that Smith (1990) scheme brings a large negative bias in cloud amount. This problem is significant also in GSM, particularly in the middle-high and high latitude.

2 Prognostic Scheme

Prognostic cloud scheme by Tiedtke (ECMWF 2004, Jakob 2000, Tiedtke 1993) has been implemented in GSM experimentally. In the scheme, time evolution of cloud water is determined by the formation and the evaporation terms which include processes of advection, heating and cooling by radiation and turbulence, heating and cooling by upward and downward motions of the air mass, detrainment from convection, evaporation by diffusion, conversion to precipitation, cloud ice fall, and so on.

Instead of a term of boundary layer cloud in Tiedtke (1993), a parameterization for subtropical marine stratocumulus (Kawai 2004, Kawai and Inoue 2006) is used in combination with Tiedtke cloud scheme on account of its effective reduction of radiation bias in such stratocumulus regions.

And cloud ice fall scheme by Kawai (2005) which enables to alleviate the time step dependence of cloud ice and represent the conversion from cloud ice to snow is also introduced in new scheme.

In the prognostic Arakawa Schubert convection

scheme used in GSM, it is assumed that mass from convection is detrained only from each cloud top of the cloud ensemble on account of calculation cost. But when the scheme is used together with the Tiedtke cloud scheme without any modifications, the anvil cloud whose origin is convection is formed at too high altitude. Therefore the detrained cloud water and the cloud amount are redistributed in a variety of altitude from cloud top to cloud base, although the function of redistribution is determined just ad hoc.

3 Result

The total cloud amount is increased in new cloud scheme (bottom panel in Figure 1) from in current scheme (top panel). Figure 2 shows correspondent errors of total cloud amount of current (top panel) and new (bottom panel) cloud schemes in which ISCCP (International Satellite Cloud Climatology Project) observation data are used as climatology. The negative bias of total cloud amount is reduced.

The increase of cloud amount is prominent at middle level in troposphere (Figure 3). In current PDF scheme, cloud amount in middle level rarely exceed 50% even inside of extratropical cyclones because of its intrinsic problem. But in prognostic Tiedtke scheme, the cloud amount can be almost 100% in such cases. This is the reason why middle level cloud amount increases in Tiedtke scheme in middle-high latitude in Figure 3. Middle level cloud is increased in tropics too. In PDF scheme middle level cloud is difficult to be formed in such region because these regions are relatively dry and cloud water from convection is evaporated in one time step. In contrast, Tiedtke scheme can represent the time evolution of cloud water. Therefore the detrained cloud is evaporated gradually and middle level cloud can be kept to some extent even in very dry condition.

The bias on OLR (Outgoing Longwave Radiation) from ERBE (Earth Radiation Budget Experiment) observational climatology is shown in Figure 4. A positive bias on OLR in current scheme (top panel) is reduced in Tiedtke scheme (bottom panel). But a positive bias on upward short wave radiation at the top of the atmosphere in tropics and subtropics is deteriorated because of excessive cloud reflection (not shown). Evaporation rate of cloud water is increased 2.5 times larger than the value used in ECMWF to suppress the cloud amount in tropics and subtropics, but the cloud in such latitude is still excessive. A treatment of cloud overlap is maybe one of factors affecting the over-reflection, and another

*e-mail : h-kawai@met.kishou.go.jp

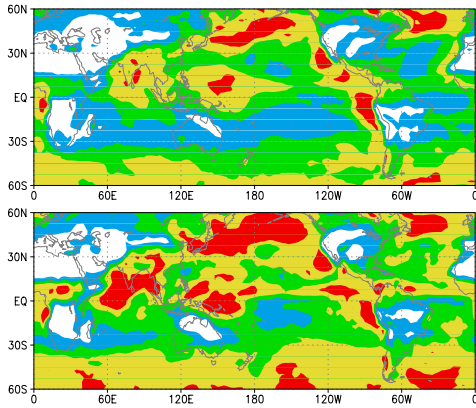


Figure 1. Total cloud amount [%] of the original (top) and the new schemes (bottom) using TL95L40. One month average from the initial time 12UTC 30 Jun 1990.

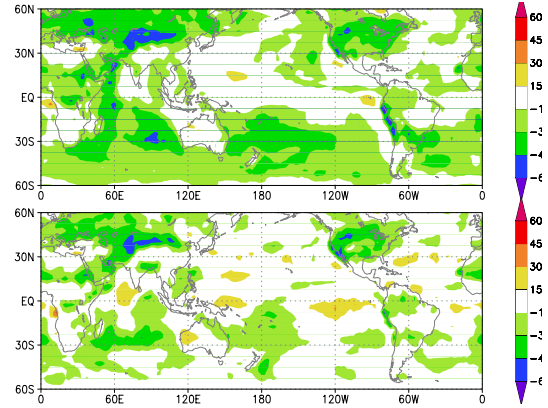


Figure 2. Same as Fig. 1 but for the error of total cloud amount based on ISCCP climatology [%].

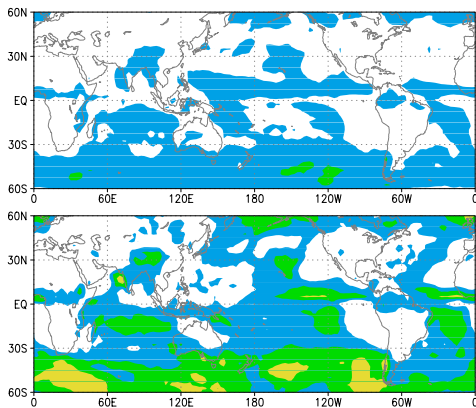


Figure 3. Same as Fig. 1 but for middle level cloud amount [%] (850hPa–500hPa).

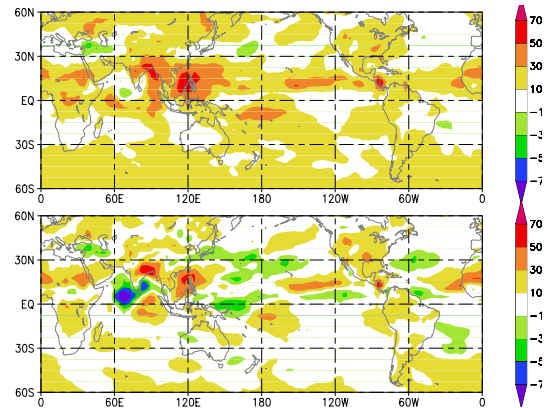


Figure 4. Same as Fig. 1 but for the error of outgoing longwave radiation $[W/m^2]$ at the top of the atmosphere based on ERBE climatology.

factor is that shallow convection parameterization is not implemented in GSM yet.

References

- European Centre for Medium-Range Weather Forecasts, 2004: IFS Documentation (CY28r1), <http://www.ecmwf.int/research/ifsdocs/CY28r1>. Part IV, Chapter 6.
- Jakob, C., 2000: The representation of cloud cover in Atmospheric General Circulation Models. A thesis submitted to the Fakultät für Physik der Ludwig-Maximilians-Universität, ECMWF.
- Kawai, H., 2004: Impact of a parameterization for subtropical marine stratocumulus. *CAS/JSC WGNE Research Activities in Atmospheric and Oceanic Modelling*, **34**, 04.13–14.
- Kawai, H., 2005: Improvement of a cloud ice fall scheme

- in GCM. *CAS/JSC WGNE Research Activities in Atmospheric and Oceanic Modelling*, **35**, 04.11–12.
- Kawai, H., and T. Inoue, 2006: A simple parameterization scheme for subtropical marine stratocumulus. *SOLA*, in press.
- Smith, R. N. B., 1990: A scheme for prediction layer clouds and their water content in a general circulation model. *Quart. J. Roy. Meteor. Soc.*, **116**, 435–460.
- Sommeria, G., and J. W. Deardorff, 1977: Subgrid-scale condensation in models of non-precipitating clouds. *J. Atmos. Sci.*, **34**, 345–355.
- Tiedtke, M., 1993: Representation of clouds in large-scale models. *Mon. Wea. Rev.*, **121**, 3040–3061.
- Wood, R., and P. R. Field, 2000: Relationships between total water, condensed water and cloud fraction in stratiform clouds examined using aircraft data. *J. Atmos. Sci.*, **57**, 1888–1905.

A Revised Radiation Scheme for Cloud Treatments in the Japan Meteorological Agency Global Spectral Model

Hiroto Kitagawa* and Shigeki Murai

Numerical Prediction Division, JMA, Tokyo, Japan

On the 7th of July 2005, a revised parameterization of cloud treatments in the radiation calculation was introduced into the operational version of the T_L319L40 GSM. In particular, the treatment of vertically overlapping clouds in the longwave part of the radiation was revised to better express cloud radiative forcings by the method of Raisanen (1998), correcting an overestimation of the top of atmosphere outgoing longwave radiation. A modified effective radius parameterization after Wyser (1998) depending on cloud temperature and water content was also introduced for ice cloud particles. In addition to these changes in radiation schemes, climatological distributions of ozone were updated.

Owing to the implementation of the revisions mentioned above, the systematic temperature errors in the stratosphere are reduced due to the updated ozone climatology (Figure 1). The positive temperature error in the upper troposphere resulting from the radiative forcing by high clouds is reduced due to the revised treatment of cloud effects in the radiation transfer. Figure 2 shows differences between simulated net shortwave / outgoing longwave radiations and satellite measurements for July 1988. Radiative fluxes at the top of atmosphere are slightly improved.

Figure 3 shows the 500 hPa geopotential height anomaly correlation scores averaged over 31 forecasts for January 2005 (left) and for August 2004 (right) in the Northern Hemisphere (upper) and Southern Hemisphere (lower). Above-described changes to the radiation parameterization of the GSM have brought about improved model performance.

References

- Raisanen, P., 1998: Effective longwave cloud fraction and maximum-random overlap of clouds: A problem and a solution. *Mon. Wea. Rev.*, 126, 3336-3340.
Wyser, K., 1998: The effective radius in ice clouds. *J. Climate*, 11, 1793-1802.

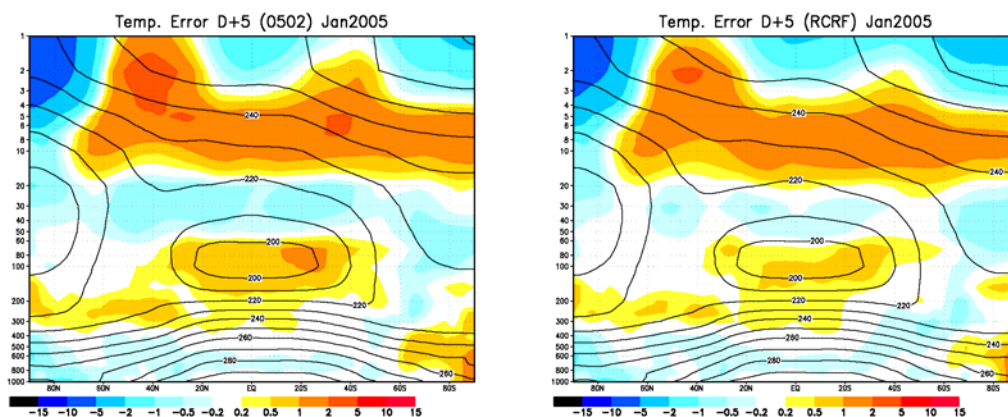


Figure 1: Zonal mean temperature structure from model forecasts (contours in K) and difference between model forecasts and verifying analyses (shading in K): the previous model (left) and the new model (right). Statistics are based on 5 days forecasts for January 2005.

* *Corresponding author address:* Numerical Prediction Division, Japan Meteorological Agency
1-3-4 Otemachi, Chiyoda-ku, Tokyo 100-8122, Japan. E-mail: kitagawa@naps.kishou.go.jp

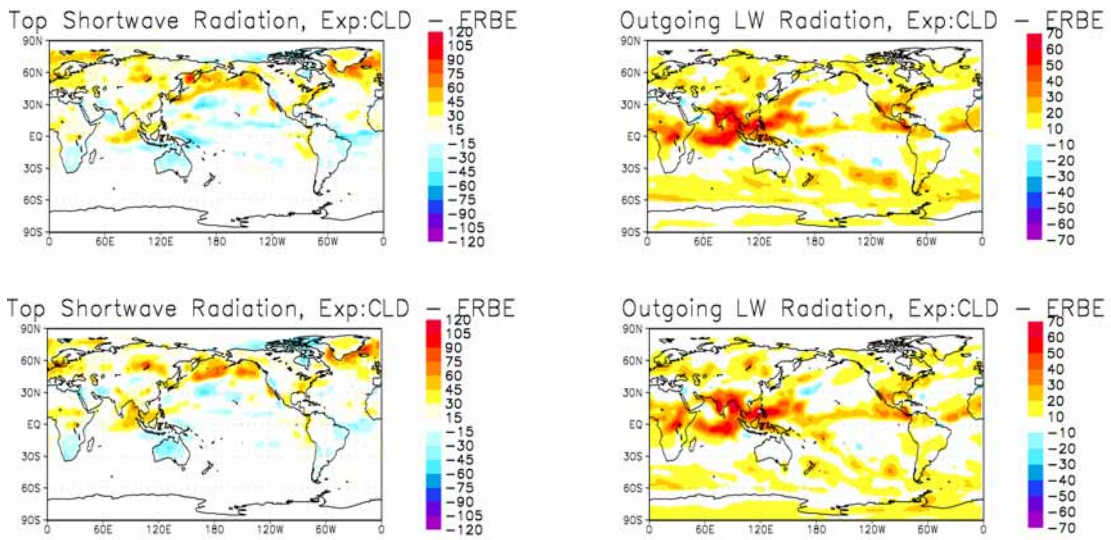


Figure 2: Difference between simulated the Top of Atmosphere Net Shortwave Radiation (left) and Outgoing Longwave Radiation (right) from ERBE data for July 1988 (unit is W/m^2), averaged over one-month forecasts using the previous model (upper) and the new model (lower).

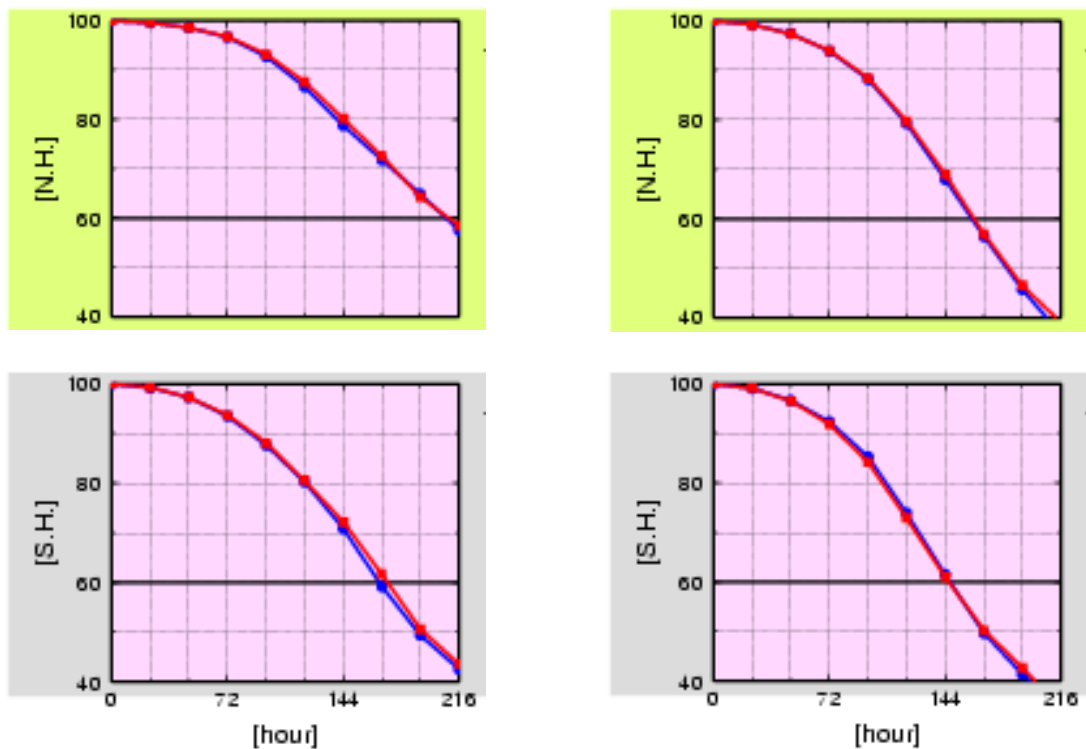


Figure 3: Anomaly correlation scores of the 500 hPa geopotential height of the Northern Hemisphere (upper) and Southern Hemisphere (lower) for 31 forecasts in January 2005 (left) and August 2004 (right) carried out with the previous operational model (blue line) and the new model (red line).

Research on the cloud radiation scheme of the JMA Non-Hydrostatic Model

Ryoji Nagasawa

Numerical Prediction Division, Japan Meteorological Agency

1-3-4 Otemachi, Chiyoda-ku, Tokyo 100-8122, Japan

E-mail: r-nagasawa@met.kishou.go.jp

The Japan Meteorological Agency Non-hydrostatic Model (NHM) has been developed for research and operational purposes. The 10-km resolution NHM has been the current operational mesoscale model since 1 September 2004, and its resolution will be increased to 5-km in March 2006. For this finer resolution model, physical processes are developed to improve overall performance of the model. Among these, developments of cloud radiation schemes are briefly described in this paper.

A sophisticated radiation scheme developed for the global spectral model of JMA (Kitagawa 2000) is implemented in the NHM since this scheme treats the cloud optical properties more properly than the current scheme developed by Sugi *et al.* (1990) does. This new scheme uses cloud properties such as cloud fraction and cloud water and ice content, which affect greatly the radiation calculation. These parameters from three methods are tested. First, the cloud fraction from predicted cloud water and ice content are directly used as in Xu and Randall (1996). Second, the cloud water content is diagnosed by a statistical relation between temperature and cloud water content (Heymsfield 1977). Third, the cloud water content is estimated from the precipitable water amount as in Hack (1998). When the methods of Heymsfield (1977) and Hack (1998) are employed, cloud fraction is diagnosed from relative humidity by a function of Ohno and Isa (1984). The following four combinations are examined. Ex4 uses the current scheme serving as a control experiment. The outline of the experiments is summarized in Table 1, and the experimental domain is shown in Fig. 1.

Ex1: Kitagawa (2000) + Xu and Randall (1996) (Xu)

Ex2: Kitagawa (2000) + Ohno and Isa (1984) + Heymsfield (1977) (Hey)

Ex3: Kitagawa (2000) + Ohno and Isa (1984) + Hack (1998) (Hack)

Ex4: Sugi *et al.* (1990) + Ohno and Isa (1984) (CTL)

Figure 2 shows Mean Error (ME) and Root Mean Square Error (RMSE), as a function of valid time, of predicted surface air temperatures verified against data from the surface observation meso-network of JMA. It shows negative (positive) bias in daytime (nighttime) in the forecasted temperatures in CTL as well as large RMSEs corresponding to this temperature bias. In Ex1, Xu-scheme reduced the greatly positive bias at nighttime, but it produces a large daytime positive bias and the associated large RMSEs. These deficiencies may be caused by the overestimation of downward shortwave radiation flux at surface because predicted cloud distribution may be less dense compared with the actual cloud distributions. With the Hey-scheme (Ex2), unlike the above-mentioned Xu-scheme, a negative bias with large magnitude as well as the corresponding large RMSEs are brought about. This may be due to the underestimation of the shortwave radiation flux at surface. The Hack-scheme (Ex3) gives almost similar results as in Ex4 (CTL) but negative bias in daytime is removed.

Figure 3 shows vertical profiles of ME and RMSE in the predicted temperature verified against sonde observations. In CTL, negative bias at around 200 hPa and positive bias at around 500 hPa are remarkable. The former may be caused by the black body cloud assumption of clouds. In the Xu-scheme, RMSE and ME are improved at most levels, but positive bias is remarkable at around 200 hPa and magnitude of RMSE at around 200 hPa is larger than CTL. This seems to be result from overestimation of predicted cloud ice content. In the Hey-scheme, negative bias at around 200 hPa is removed, but positive bias at around 500 hPa is not removed. With the Hack-scheme, negative bias at around 200 hPa and positive bias at around 500 hPa are improved to some extent; in terms of RMSE, improvement above 700 hPa is remarkable.

According to the experiments Ex1-4, it was found that the Hack-scheme gives reasonable results in the prediction of temperatures at the surface and aloft. Thus this scheme will be adopted for the radiation scheme in the 5-km resolution operational mesoscale model. This scheme is, however, somewhat rude in diagnosing the cloud fraction, an important parameter in the cloud radiation calculation. Since the results of the experiments indicate that the cloud radiation calculation greatly depends on the cloud distribution and the cloud water content, refinement of cloud diagnosing method and effective use of model-predicted cloud variables remain for future work.

References

Hack, J. J., 1998: Sensitivity of the simulated climate to a diagnostic formation for cloud liquid water. *J. Climate*, **11**, 1497-1515.

Heymsfield, A. J., 1977: Precipitation development in stratiform ice clouds: A micro-physical and dynamical study. *J. Atmos. Sci.*, **34**, 367-381.

Kitagawa, H., 2000: Radiation scheme. *Report of Numerical Prediction Division*, **46**, 16-31 (in Japanese, Suuchiyouhouka Bessatsu Houkoku).

Ohno, H. and M. Isa, 1984: A statistical relation between GMS-viewed cloud amount and relative humidity. *Tenki*, 31, No.8, 493-495 (in Japanese).

Sugi, M., K. Kuma, K. Tada, K. Tamiya, N. Hasegawa, T. Iwasaki, S. Yamada and T. Kitade, 1990: Description and Performance of the JMA operational global spectral model (JMA-GSM88). *Geophys.Mag*, **43**, 105-130.

Xu, K. M., and D. A. Randall, 1996: A Semiempirical Cloudiness Parameterization for Use in Climate Models. *Journal of the Atmospheric Sciences*, **53**, 3084-3102.

Table. 1 Outline of the experiments

Experimental period	From 7 to 8 Jun 2004 From 12 to 13 Jul 2004 From 16 to 17 Jul 2004 From 27 to 29 Sep 2004
Initial times	00, 06, 12, 18 UTC
Integration time	15 hours
Horizontal resolution	5km
Vertical layers	50
Initial condition	Operational meso analysis
Lateral boundary condition	Forecasts of Regional Spectral Model

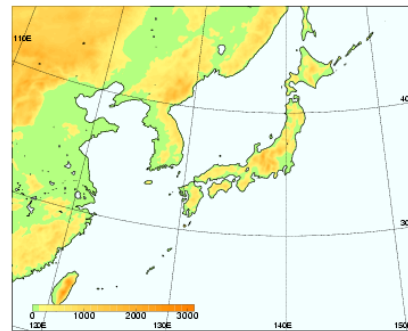


Fig. 1 Forecast domain for the experiments

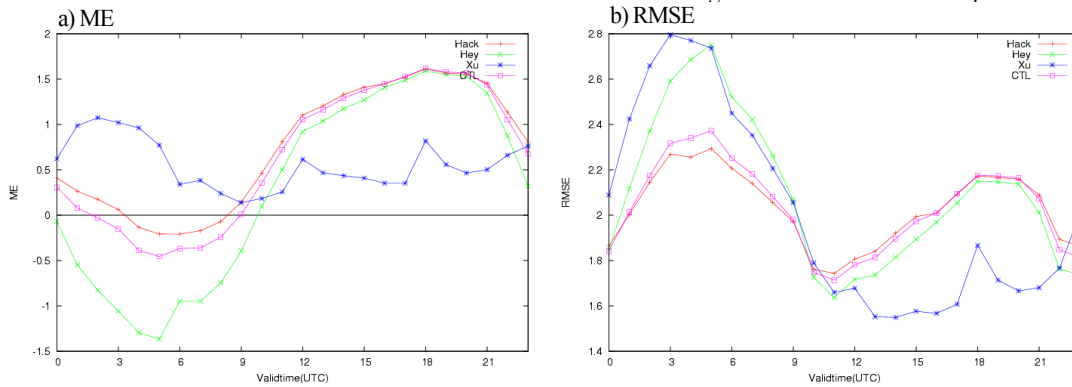


Fig. 2 a) ME and b) RMSE, as a function of valid time, of the surface air temperatures predicted by various input clouds verified against date from the surface observations network of JMA.

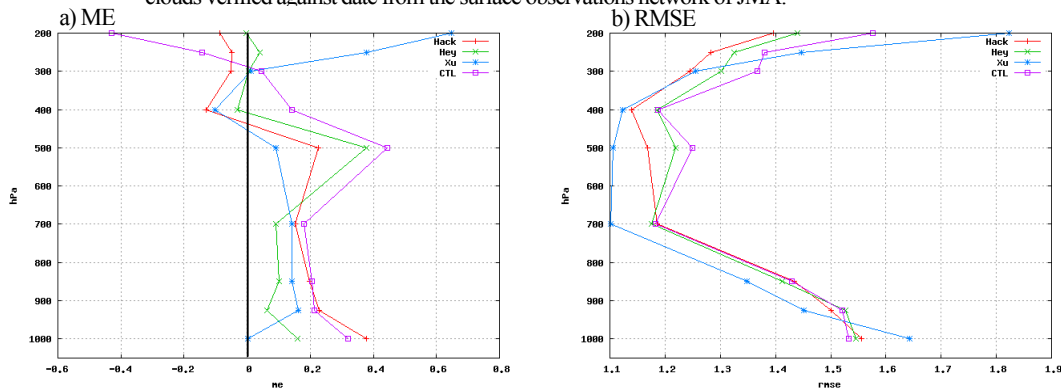


Fig. 3 Vertical profiles of a) ME and b) RMSE in the temperature predicted by various clouds verified against sonde observations. The data at 54 observational points included in the computational domain are used.

Development of cumulus parameterization scheme in the non-hydrostatic mesoscale model at the Japan Meteorological Agency

Shiro Ohmori and Yoshinori Yamada

Numerical Prediction Division, Japan Meteorological Agency

1-3-4 Otemachi, Chiyoda-ku, Tokyo 100-8122, Japan

E-mail: s-ohmori@met.kishou.go.jp

1. Introduction

The Japan Meteorological Agency non-hydrostatic model (hereafter JMANHM) has been used for operational mesoscale model with a horizontal resolution of 10-km since September 2004 (Saito et al., 2005). The moist process is a combination of a three-class bulk microphysical modeling and the Kain Fritsch cumulus parameterization scheme (Kain and Fritsch, 1990; Kain, 2004, hereafter K-F scheme). Since the K-F scheme has a large impact on the precipitation forecast, several parameters in the scheme were adjusted so that the precipitation forecast becomes better (Yamada, 2003; Ohmori and Yamada, 2004).

The horizontal resolution of the operational mesoscale model will be enhanced to be 5-km from March 2006. Even in the 5-km resolution model, the K-F scheme is still used for better precipitation forecasts. With the important parameters adjusted for the current 10-km resolution model, the K-F scheme may, however, not work well at 5-km resolution. In this paper, we will describe results of refinements of the K-F scheme for the 5-km mesoscale model.

2. Control Experiment with the same setting as horizontal resolution 10-km

First of all, we have examined the performance of precipitation forecasts of the 5-km resolution model with the same parameters in the K-F scheme as those for the current 10-km resolution model. As indicated by statistical verification scores (Fig. 1), the accuracy of precipitation forecast of the 5-km resolution model is almost the same as that of the current mesoscale model, suggesting that a fine tuning of the K-F scheme is required. In the following, we show the result of sensitivity experiment on the three important parameters in the K-F scheme in order to improve precipitation forecasts.

3. Important parameters of K-F scheme

a. Threshold of condensates to convert into precipitation

In the K-F scheme a Kessler-type precipitation formation is adopted such that condensates in the updraft are converted into precipitation when their amount exceeds a prescribed threshold value. The increase in this threshold from $8.0 \times 10^{-4} \text{ kg kg}^{-1}$ in the 10-km resolution model to $2.0 \times 10^{-3} \text{ kg kg}^{-1}$ ameliorates the representation of the occurrence of weak rain (around a few millimeters per three hours) in summer season. The resultant effect is the increase in threat scores due to the reduction in the false alarm.

b. The life time of deep convection

The K-F scheme assumes that the convection consumes the convective available potential energy (CAPE) in a certain time scale. This time scale lying within 1800 to 3600 seconds is used to determine the heating and moistening ratios, and is based on the advective time scale. The original formulation of the K-F scheme has tendency to assign this time scale of 1800 seconds for a fine mesh model with horizontal resolution $< 10 \text{ km}$. A shorter time scale of 900 seconds improved the three-hourly accumulated precipitation forecast by increasing the occurrence frequency at rain rate around 20 millimeters per three hours.

c. The life time of shallow convection

The K-F scheme also includes the shallow convection other than deep convection. The shallow convection produces non-precipitable condensates and no precipitation. The shallowness of the convection is determined by a vertical extent of the cloud layer that is given by a function of temperature at lifting condensation level of rising air parcel. A time scale is also prescribed as in the deep convection.

The importance of the time scale for shallow convection has appeared in the precipitation forecasts during cold air outbreaks of winter monsoon. Under these conditions, shallow convective clouds developed over the sea bring about precipitation. With a default value of 2400 seconds, the band-shaped weak rain is sometimes excessively reproduced to degrade the statistical verification scores. With a shorter life time of 600 seconds, the excessive weak rain is ameliorated well (Fig. 2).

4. Forecast experiments

With the fine-tuned K-F parameters mentioned above, experiments with the 5-km resolution

model are made for both summer (June and July 2004) and winter (December 2004 and January 2005) seasons to investigate the performance of the precipitation forecast to be evaluated by statistical verification scores.

a. Summer season

The threat scores at all rain rates are larger than those from the current 10-km model. Taking into account that the bias scores of 5-km model is much close to unity, it is clear that the overall performance of precipitation forecasts of the 5-km is improved (Fig. 1).

b. Winter season

Both bias and threat scores from 5-km resolution model were comparable at all rain rates, unlike the summer season (not shown). The enhancement of the horizontal resolution did not bring about sizable improvements. One reason of this may in part be explained in terms of the smaller spatial scale of convection in cold season relative to that in summer time. The horizontal resolution of 5-km seems to be still much larger than the spatial scale of the convective clouds in cold season.

5. Future Plan

In 2007, the 5-km resolution mesoscale model is planned to be operated up to 33 forecast hours, the current operational being up to 15 hours. Fine tuning of the K-F scheme for such prolonged forecasts may be necessary for better precipitation forecast.

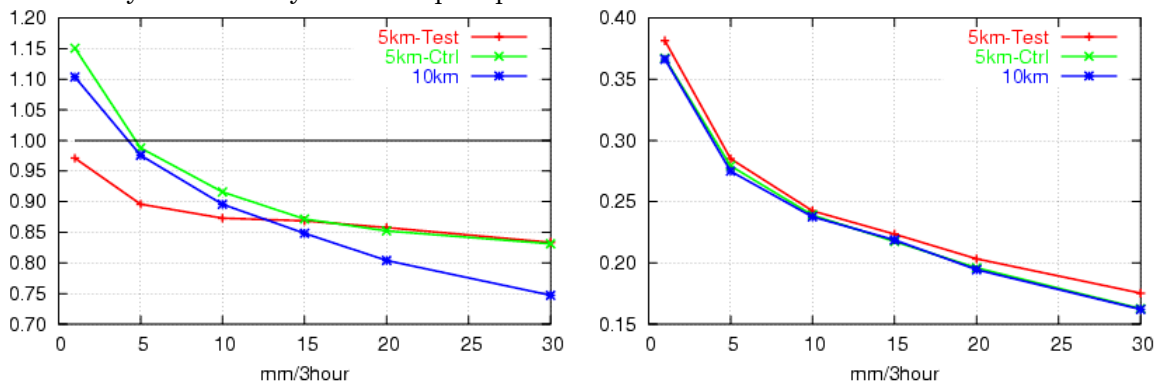


Fig. 1 The bias scores (left) and threat scores (right) against the radar rain gauge composite data. The experiment periods are 6-12th June, 20-26th June and 7-20th July 2004. Red, green and blue lines mean the result from optimized 5-km experiment, that from pre-optimized 5-km experiment and that from 10-km experiment, respectively.

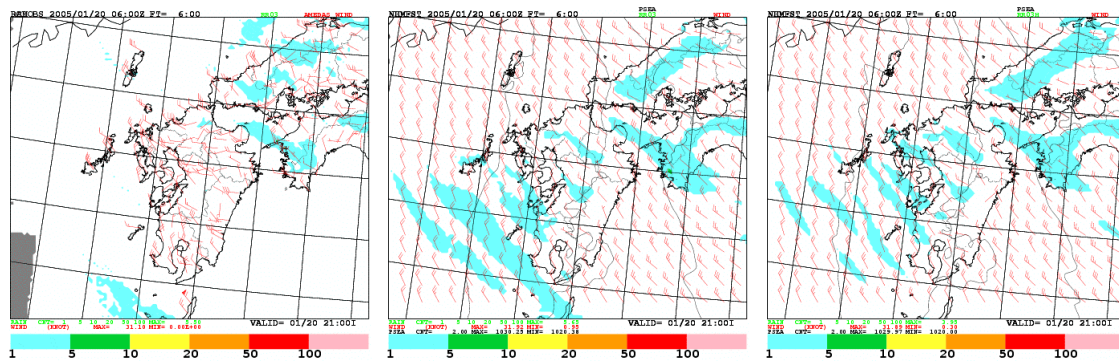


Fig. 2 Observed rain and wind at 20th January 2005 12UTC (left) and the results of 6 hours forecast with 5-km horizontal resolution. The shallow cumulus life time is 2400 seconds (center) and 600 seconds (right). Initial time of forecast is 20th January 2005 06UTC. Rain rates are in millimeter per three hours.

References:

Kain, J.S., and J.M. Fritsch, 1990: A one-dimensional entraining/detraining plume model and its application in convective parameterization. *J. Atmos Sci*, 47, 2784-2802.
 Kain, J.S., 2004: The Kain-Fritsch Convective Parameterization: An Update. *J. Appl Meteor*, 43, 170-181
 Ohmori, S. and Y. Yamada, 2004: Implementation of the Kain-Fritsch Convective Parameterization scheme in JMA's Non-hydrostatic Model. *CAS/JSC WGNE Research Activities in Atmospheric and Oceanic Modelling*, 33, 04, 25-26
 Saito, K., T. Fujita, Y. Yamada, J. Ishida, Y. Kumagai, K. Aranami, S. Ohmori, R. Nagasawa, S. Kumagai, C. Muroi, T. Kato, H. Eito, and Y. Yamazaki, 2005: The Operational JMA Nonhydrostatic Mesoscale Model. *Submitted to Mon. Wea. Rev.*
 Yamada, Y. 2003: Cumulus Convection Schemes. *Suuchiyohou-ka Houkoku Bessatsu* 49, 84-89.(in Japanese)

Sensitivity to Graupel Particle Properties in LMK Simulations With a Three-Category Ice Scheme

Thorsten Reinhardt and Axel Seifert
Deutscher Wetterdienst, Kaiserleistr. 35, D-63067 Offenbach, Germany
E-mail: Thorsten.Reinhardt@dwd.de

Introduction

For DWD's mesoscale limited-area model LM, an additional optional microphysical parameterization scheme which takes into account also graupel has been developed (Reinhardt, 2005). This scheme is an extension of DWD's currently operational microphysics scheme (Doms et al., 2005) which is used in the global model GME (40 km mesh size) and in LM (7 km mesh size). It considers the mixing ratios of cloud water, cloud ice, rain, snow, and graupel as prognostic condensate categories. It is intended to be used in LMK ("LM-Kürzestfrist", see Doms and Förstner, 2004), the convection-resolving short-range version of LM.

Sensitivity to Graupel Particle Properties

Gilmore et al. (2004) carried out sensitivity tests with respect to the assumed properties of the graupel/hail category within a bulk (one-moment) microphysics parameterization. They used an idealized convective environment for their model setup (1 km mesh size, 30 m/s and 50 m/s wind speed with veering wind shear, supercell development, similar to Weisman and Klemp, 1984) and varied the intercept parameter N_0^g of the graupel particle size distribution ($f(D) = N_0^g \exp(-\lambda D)$) and the graupel particle density ρ_g . Decreasing N_0^g as well as increasing ρ_g each changes the bulk properties of the particle ensemble towards more hail-like properties, e.g. faster sedimentation and less rapid melting. In general, more precipitation accumulated at ground was found in the cases with the graupel/hail category weighted towards large hail.

The question arises whether underprediction of precipitation in convective events seen in a number of cases simulated with LMK may be caused by the lack of high-density hail-like ice particles in the microphysical parameterization scheme.

Sensitivities similar to those seen by Gilmore et al. (2004) could also be found with LMK in a similar idealized 3-d convective setup (2.8 km mesh size, unidirectional wind shear only, wind speed 25 m/s, symmetric storm splitting, similar to Weisman and Klemp, 1982). Surface precipitation (both mean and maximum) tends to be higher with the graupel category weighted towards hail-like properties, i.e. smaller intercept parameter and larger particle density, see Table 1. For $\rho_g = 0.4 \text{ g/cm}^3$ and $\rho_g = 0.9 \text{ g/cm}^3$, the velocity-size relationship is taken from Lin et al. (1983) and is considered in all microphysical process rates. A large sensitivity to N_0^g is found in the $\rho_g \approx 0.2 \text{ g/cm}^3$ and $\rho_g = 0.4 \text{ g/cm}^3$ cases: With N_0^g decreasing from $4 \times 10^6 \text{ m}^{-4}$ to $4 \times 10^4 \text{ m}^{-4}$ total surface precipitation increases by 144 % and 73 %, resp. Higher mass-weighted sedimentation velocity of the graupel particle ensemble (i.e. smaller N_0^g) makes the particles less susceptible to horizontal advection (and subsequent evaporation outside the storm) and can therefore lead to more surface precipitation. As to be expected, with decreasing N_0^g and increasing ρ_g more unmelted graupel/hail can reach the ground. Much less surface precipitation (compared to all simulations including graupel) is found in the no-graupel (= standard LM microphysics) case confirming the need of a faster-than-snow falling ice species when simulating severe convection.

Less sensitivity is found in two simulations of real (convective) weather situations: A pre-frontal squall-line case (July 18, 2004) and a case with less organized, more isolated convection in a situation with weak large-scale gradients (August 07, 2004), see Tab. 2. In contrast to the idealized warm-bubble setup, in the August 07 case area-mean precipitation tends to decrease when moving from light-graupel to hail-like particle properties in the graupel/hail category, while in the July 18 case one might see the same but very much damped tendency as in the idealized setup. As in the idealized setup, in both real cases maximum precipitation is lower in the no-graupel simulation than in any of the simulations including graupel. In the August 07 case simulated precipitation becomes less widespread (i.e. areas receiving precipitation becoming smaller without maxima being reduced) when moving from the no-graupel over the low-density-graupel to the high-density-graupel/hail case which might be due to the effect of ice precipitation becoming less subject to horizontal advection when sedimenting faster (no figure shown). In the July 18 case, this feature is not seen. That the sensitivity to the assumed properties of the graupel category is smaller in simulations of real convective cases compared to the idealized setup may be attributed (i) to more (negative) feedbacks being active in longer integration time and on a larger domain, (ii) to graupel being overall less important in simulations of real weather events (since there are always also more stratiform and snow-dominated areas) compared to the idealized simulations where much more graupel than snow is simulated, and (iii) to significant decrease of depositional growth when graupel is assumed to be more hail-like opposed to riming being less affected. Tab. 2 shows also that in simulations weighted towards large hail (all $N_0^g = 4 \times 10^4 \text{ m}^{-4}$ simulations; the more the higher ρ_g) explicit simulation of hail occurrence at the ground is possible.

N_0^g	ρ_g	TotP	TotG	MaxP	MaxG
4×10^4	≈ 0.2	36.17	0.1069	23.03	0.0001
4×10^5	≈ 0.2	27.55	0.0000	16.91	0.0000
4×10^6	≈ 0.2	14.80	0.0000	10.91	0.0000
4×10^4	0.4	35.51	0.1883	22.79	0.5017
4×10^5	0.4	32.02	0.0000	19.07	0.0000
4×10^6	0.4	25.79	0.0000	16.05	0.0000
4×10^4	0.9	32.82	3.4673	25.56	5.8234
4×10^5	0.9	35.01	0.0000	21.27	0.0000
no graupel	–	4.13	–	4.26	–

Table 1: Comparison of surface precipitation for simulations with different assumed intercept parameter N_0^g (in m^{-4}) and graupel particle density ρ_g (in g/cm^3). Accumulated mass on ground (total precipitation (TotP) and graupel (TotG) in Tg and maximum total precipitation (MaxP) and maximum graupel precipitation (MaxG) in mm. All after 2 hours.

N_0^g	ρ_g	Aug 07, 2004				Jul 18, 2004			
		MeanP	MeanG	MaxP	MaxG	MeanP	MeanG	MaxP	MaxG
4×10^4	≈ 0.2	0.3627	0.0004	64.05	0.46	4.384	0.222	91.37	1.65
4×10^5	≈ 0.2	0.4461	0.0000	57.64	0.00	4.318	0.0	94.46	0.0
4×10^6	≈ 0.2	0.4548	0.0000	47.71	0.00	4.183	0.0	81.20	0.0
4×10^4	0.4	0.3136	0.0002	49.55	1.07	4.369	2.098	98.34	3.15
4×10^5	0.4	0.4023	0.0000	58.61	0.00	4.341	0.0	83.31	0.0
4×10^6	0.4	0.4846	0.0000	57.92	0.00	4.341	0.0	83.71	0.0
4×10^4	0.9	0.3109	0.0061	73.71	10.15	4.276	20.906	98.39	9.60
4×10^5	0.9	0.3129	0.0000	56.61	0.05	4.334	0.047	86.73	0.0
no graupel	–	0.4190	–	41.96	–	4.154	–	79.41	–

Table 2: As Tab. 1, but for simulated 23-hour precipitation sum of LMK forecasts started at August 07, 2004 00 UTC and at July 18, 2004 00 UTC. MeanP and MeanG stand for mean total precipitation and mean graupel precipitation (in mm), resp. Numbers are valid for a subdomain of total model domain.

Conclusion and Outlook

Underprediction of convective precipitation cannot be cured by changing the graupel particle properties from those of low-density graupel to those of more hail-like particles (at least in the 3-d simulations of real cases). However, it is under consideration to change the bulk properties of the graupel category in such way that more hail-like particles instead of low-density graupel particles are represented. This would allow for an explicit simulation of surface hail occurrence. Then it would be more consistent to take into account also wet growth of the hailstones which is neglected currently. On the other hand, medium- and low-density graupel would then be represented less accurately. A compromise might be to make N_0^g dependent on the graupel/hail mixing ratio, i.e. let N_0^g decrease when q_g increases.

References

- Doms, G. and J. Förstner, 2004:** Development of a kilometer-scale NWP-system: LMK. *COSMO Newsletter*, 4, 159–167.
- Doms, G. et al., 2005:** A Description of the Nonhydrostatic Regional Model LM. Part II: Physical Parameterization. DWD, GB Forschung und Entwicklung.
- Gilmore, M. S., J. M. Straka, and E. N. Rasmussen, 2004:** Precipitation uncertainty due to variations in precipitation particle parameters within a simple microphysics scheme. *Mon. Wea. Rev.*, 132, 2610–2627.
- Lin, Y.-L., R. D. Farley and H. D. Orville, 1983:** Bulk parameterization of the snow field in a cloud model. *J. Climate Appl. Meteor.*, 22, 1065–1092.
- Reinhardt, T., 2005:** A prognostic graupel microphysics scheme for high-resolution NWP. The WGNE Blue Book 2005.
- Weisman, M. L. and J. B. Klemp, 1982:** The dependence of numerically simulated convective storms on vertical wind shear and buoyancy. *Mon. Wea. Rev.*, 110, 504–520.
- Weisman, M. L. and J. B. Klemp, 1984:** The structure and classification of numerically simulated convective storms in directionally varying wind shears. *Mon. Wea. Rev.*, 112, 2479–2498.

Sensitivity of near surface temperature model errors to the introduction of a prognostic snow density and a revised formulation of snow heat conductivity

**Bodo Ritter, Deutscher Wetterdienst, P.O.Box 106465, 63004 Offenbach am Main
Germany**

In the presence of snow on the ground the diurnal evolution of surface and near surface temperatures is governed not only by the forcing due to radiative and turbulent fluxes and the soil heat flux. In addition, heat conduction through the snow layer becomes important in situations when the soil surface temperatures deviate significantly from the values at the top of the snow layer. The contribution of this process to the energy budget at the interface between atmosphere and snow surface is controlled by the thickness of the snow layer and the associated heat conductivity.

In early spring 2005 the operational global model of DWD assumed a constant snow density of 250 kg/m^3 and a heat conductivity of approximately 0.2 W/(m K) with a weak dependence on the total water content of the snow layer. With these assumptions the decoupling of the snow surface from the underlying soil was overly efficient, leading to an excessive cooling at the snow surface at night and a corresponding error in near surface minimum temperatures. Fig.1a illustrates the distribution of near surface temperatures for a situation when a snow layer had been present for several days in most parts of Germany. Compared to observations the model was frequently too cold by more than 5 K. Overall the model simulated temperatures exhibited an excessive diurnal cycle above the snow. A revision of the formulation for the snow heat conductivity in conjunction with the introduction of a prognostic snow density alleviated the problem considerably. Snow heat conductivity is determined following the approach of Yen (1981) as a function of snow density. The impact of ageing on the density of existing snow itself follows the formulation proposed by Verseghy (1991). Even though the simulation of the snow density accounts for the metamorphosis of existing snow and the impact of freshly falling snow only in a very crude way, the formulation captures important aspects of the temporal evolution such as compaction due to processes like gravitational sedimentation and the reduction of the mean density, should fresh snow fall on an existing snow layer. Fig.1b illustrates the impact of these changes on the simulated nighttime temperatures. Compared to the operational model considerably higher temperatures were predicted and a better agreement with observations was achieved.

Despite these improvements the model still exhibits a significant negative temperature bias in wintertime situations when the atmosphere is characterised by a stable stratification near the surface. The remaining bias appears to be related to other model deficiencies since sensitivity experiments with further modifications affecting the heat flow through the snow layer had no significant impact on the problem. Further investigations will be performed with the turbulence scheme as a focal point of interest since the simulation of the stable boundary layer is generally a critical issue in NWP models.

References

Verseghy, D.L., 1991: CLASS – a Canadian Land Surface Scheme for GCMs. 1. Soil model. *Int.J.Climatology*, 11, 111-113

Yen, Y.-C., 1981: Review of thermal properties of snow, ice and sea ice. CCREL Rep.81-10, Cold Reg. Res. and Eng. Lab., Hanover, N.H.

{ T_2M K 2005030312 + 018h DWD } + -273.15
mean: -13.13 std: 3.61 min: -19.62 max: -2.05

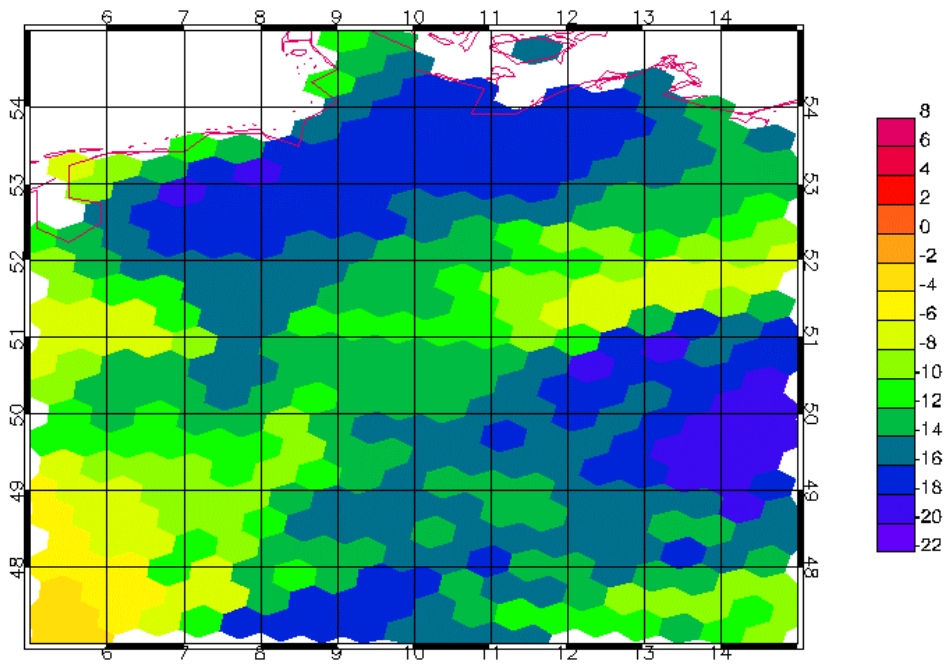


Fig.1a: Simulated near surface temperatures (°C) with operational model version for Central Europe based on initial data from March 3rd 2005 12 UTC

{ T_2M K 2005030312 + 018h DWD Expld:05347 } + -273.15
mean: -11.52 std: 2.92 min: -16.87 max: -1.27

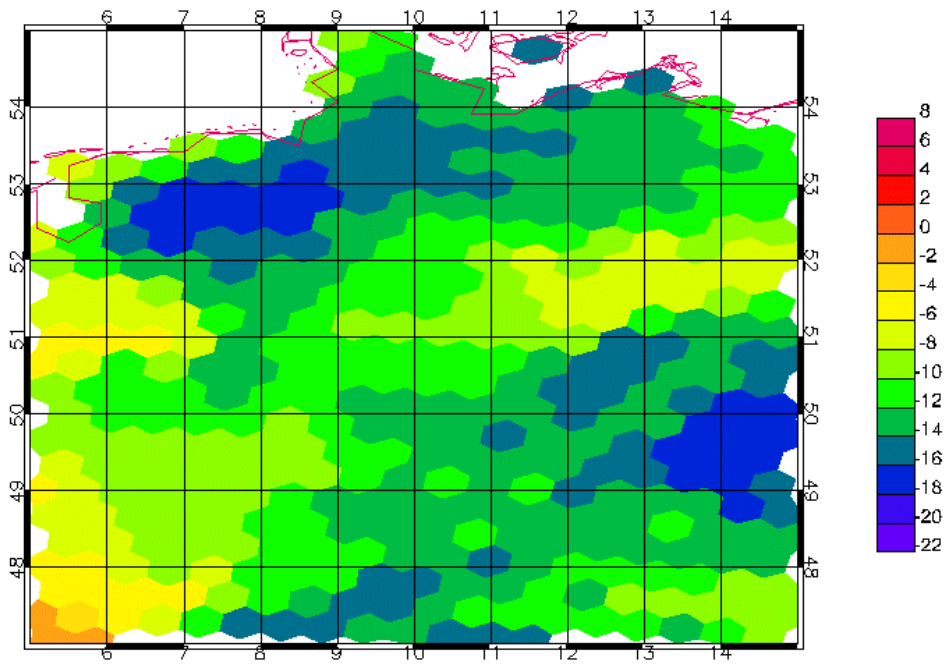


Fig.1b: Simulated near surface temperatures (°C) with experimental model version for Central Europe based on initial data from March 3rd 2005 12 UTC

Effect of Turbulence on Atmospheric Chemistry for non-constant reaction rate.

Volf Shnaydman and Georgiy Stenchikov

Department of Environmental Sciences, Rutgers University, New Brunswick, NJ, USA

volf@envsci.rutgers.edu

The transport equation for N reacting species q_i

$$\frac{\partial q_i}{\partial t} + u_\alpha \frac{\partial q_i}{\partial x_\alpha} = \alpha_{ij} q_i q_j \quad (1)$$

contains a right-hand-side non-linear term responsible for chemical transformations. α_{ij} are elements of a symmetric matrix of rates of chemical reaction between species i and j . Summation is conducted on all repeating indexes. Index α equal to 1, 2, 3 and indexes i and j change from 1 to N. In /Shnaydman, Stenchikov,2005/ we assume that chemical rate transformations α_{ij} are constant.

Now we developed the closure scheme of mean concentration calculation for the case when rate reaction depends on temperature. For the simplicity we suppose that the reaction rate is a linear function of the temperature

$$\alpha_{ij} = \alpha_0 (T/T_0). \quad (2)$$

The application of the Reynolds averaging leads to the following transport-diffusion equation

$$\frac{\partial \bar{q}_i}{\partial t} + \bar{u}_\alpha \frac{\partial \bar{q}_i}{\partial x_\alpha} = \frac{\partial}{\partial x_\beta} K_L \frac{\partial \bar{q}_i}{\partial x_\beta} + \frac{\partial}{\partial x_3} K_Z \frac{\partial \bar{q}_i}{\partial x_3} + \quad (1) \quad (2)$$

$$\frac{\partial}{\partial x_\alpha} \gamma \frac{\partial \bar{q}_i}{\partial x_\alpha} - \alpha_0 (\bar{T}/T_0) (\bar{q}_i \bar{q}_j) + \alpha_0 (\bar{T}/T_0) (\overline{q'_i q'_j}) - \quad (3)$$

$$\frac{\alpha_0}{T_0} (\overline{T' q'_i \bar{q}_j} + \overline{T' q'_j \bar{q}_i} + \overline{T' q'_i q'_j}) \quad (4)$$

The effect of turbulence on the temporal evolution of mean concentration is given by the vertical (1) and horizontal (2) diffusion, chemical interaction between reacting species(3) and temperature influence on the reaction rate in the turbulent environment.

The input heat equation for potential temperature and transport-diffusion mean concentration equations are used for definition of mixed temperature-concentration covariance. and the temperature variance

$$\frac{\partial \overline{T' q'_i}}{\partial t} + \bar{u}_\alpha \frac{\partial \overline{T' q'_i}}{\partial x_\alpha} = \frac{\partial}{\partial x_\beta} K_L \frac{\partial \overline{T' q'_i}}{\partial x_\beta} + \frac{\partial}{\partial x_3} K_Z \frac{\partial \overline{T' q'_i}}{\partial x_3} +$$

$$2(K_L \frac{\partial \bar{q}_i}{\partial x_\beta} \frac{\partial \bar{T}}{\partial x_\beta} + K_Z \frac{\partial \bar{q}_i}{\partial x_3} \frac{\partial \bar{\theta}}{\partial x_3}) - \alpha_0 (\overline{\bar{q}_i T' q'_j} + \overline{\bar{q}_j T' q'_i}) + \frac{\alpha_0}{T_0} (\overline{T'^2 \bar{q}_i \bar{q}_j}) - \quad (1)$$

$$\alpha_0 (\overline{T' q'_i q'_j}) - \frac{\alpha_0}{T_0} (\overline{T'^2 q'_i \bar{q}_j} + \overline{T'^2 q'_j \bar{q}_i}) - \frac{\alpha_0}{T_0} (\overline{T'^2 q'_i q'_j}), \quad (4)$$

(2)

In (4) the additional terms related with temperature variance (1), third and fourth mixed moments (2) are appeared. The first additional term is defined by using the equation of temperature variance.

$$\frac{\partial \overline{T'^2}}{\partial t} + \bar{u}_\alpha \frac{\partial \overline{T'^2}}{\partial x_\alpha} = \frac{\partial}{\partial x_\beta} K_L \frac{\partial \overline{T'^2}}{\partial x_\beta} + \frac{\partial}{\partial x_3} K_Z \frac{\partial \overline{T'^2}}{\partial x_3} + 2(K_L \frac{\partial \bar{T}}{\partial x_\beta} \frac{\partial \bar{T}}{\partial x_\beta} + K_Z \frac{\partial \bar{\theta}}{\partial x_3} \frac{\partial \bar{\theta}}{\partial x_3}) \quad (5)$$

Follow /Petersen et. al./, we wrote the closure parameterization for the third and fourth moments.

$$\begin{aligned} \overline{q'_i q'^2_j} &= C \tau (\overline{u'_\alpha q'_i} \frac{\partial q'^2_j}{\partial x_\alpha} + u'_\alpha q_j \frac{\partial \bar{q}_i}{\partial x_\alpha}) \\ \overline{T' q'_i q'_j} &= -C \tau (\overline{u'_\beta T'} \frac{\partial q'_i q'_j}{\partial x_\beta} + \overline{u'_3 q'} \frac{\partial q'_i q'_j}{\partial x_3} + \overline{u'_\alpha q'_i q'_j} \frac{\partial \bar{T}}{\partial x_\alpha}) \\ \overline{T'^2 q'_i} &= -C \tau (\overline{u'_\beta T'} \frac{\partial T' q'_i}{\partial x_\beta} + \overline{u'_3 \theta'} \frac{\partial T' q'_i}{\partial x_3} + \overline{u'_\alpha T' q'_i} \frac{\partial \bar{T}}{\partial x_\alpha}) \quad \tau = E / \varepsilon \\ \overline{T'^2 q'_i q'_j} &= -C \tau (\overline{u'_\alpha T'^2} \frac{\partial q'_i q'_j}{\partial x_\alpha} + \overline{u'_\alpha q'_i q'_j} \frac{\partial \overline{T'^2}}{\partial x_\alpha}) \end{aligned} \quad (6)$$

$$\tau = E / \varepsilon, \quad - \overline{u'_i S'} = K_m \frac{\partial \bar{S}}{\partial x_i} \quad S = q_i, q_j, T, \text{ their variances, second, third and fourth}$$

moments, $K_m = K_L$, if $i=1,2$ and $K_m = K_Z$, $T = \theta$ if $i=3$

where E is the turbulent kinetic energy and epsilon is the dissipation rate. These values are obtained from two-equation closure scheme/Shnaydman, 2004 / based on the turbulent kinetic energy and dissipation rate prediction equations.

The developed model of the transport and turbulent diffusion of reacting species together with improved two-equation turbulence closure scheme including the main mechanisms of spreading the pollutants will be applied for estimation of atmospheric pollution characteristics.

Petersen, A.C., Beets, C.H., H.van Dop, Duynkerke, P.G., Siebesma, A.P., Mass-flux characteristics of reactive scalars in the convective boundary layer. *J. Atmos. Sci.*, 56, 37-56, 1999.
Shnaydman, V., Improved hydrodynamical scheme of the turbulence description, *Res. Act., Atmospheric and Oceanic Modeling, WMO*, 34, 5-14, 2004.

Shnaydman, V., Stenchikov, G., Effect of Turbulence on Atmospheric Chemistry, *Res. Act., Atmospheric and Oceanic Modeling, WMO*, 35, 4-29, 2005.